Tug of War at Air-Water Interface: Understanding Lipid-Nanoparticle and Lipid-Protein Interaction Associated With Lung Surfactants at a Molecular Level

By

Aishik Chakraborty

Submitted to the graduate degree program in Chemical & Petroleum Engineering and the Graduate Faculty of the University of Kansas in partial fulfillment of the requirements for the degree of Master of Science.

_____

Chairperson: Dr. Prajnaparamita Dhar

_____

Dr. Stevin Gehrke

_____

Dr. Kevin Leonard

Date Defended: 5.15.15

The Thesis Committee for Aishik Chakraborty

certifies that this is the approved version of the following thesis:

Tug of War at Air-Water Interface: Understanding Lipid-Nanoparticle and Lipid-Protein Interaction Associated With Lung Surfactants at a Molecular Level

_____

Chairperson: Dr. Prajnaparamita Dhar

Date approved: 5.15.15

Abstract

Lung surfactants [LS] are a complex mixture of lipids and proteins that line the air-water interface in the alveoli of the lungs. They lower the work of breathing by reducing the surface tension and also form a line of defense against particles small enough to enter the respiratory tract. A deficiency of LS may lead to the fatal Neonatal Respiratory Distress Syndrome [NRDS] in premature infants, whereas, an impairment may cause Acute Respiratory Distress Syndrome [ARDS], irrespective of the age. Medical intervention in the form of Surfactant Replacement Therapy [SRT] becomes a lifesaver in such cases. Developing synthetic LS with efficacy in treating ARDS has therefore been a focus of this work. Further, with the rapid development in commercial and biomedical applications of engineered nanoparticles (ENPs), concerns regarding the effect of inhaled nanoparticles on LS function also need to be addressed. In this work, we have used a carbon-based ENP to understand their interactions with model LS. Our studies revealed that the alkyl chain saturation and head group charge of the phospholipids that form the major components of the LS play modulate phospholipid-nanoparticle interactions. We monitored the effect of Engineered Carbon Nanodiamonds [ECN] on five lipid compositions. In a zwitterionic environment, the nanoparticle was line active and favored the phospholipid domain boundaries. However, in an anionic environment, the nanoparticles reduced the packing density between domains. The electrostatic charge interaction was found to be more dominant.

We also observed the tug of war between a synthetic surfactant protein (analog of natural surfactant protein, SPB) called MiniB and cholesterol. MiniB increased the line tension of the domains whereas cholesterol reduced the same. MiniB also helped in forming reversible collapse at low surface tension, which in turn saved material loss to the bulk. A lower concentration of both proved to be effective in increasing the surface activity of LS.

Acknowledgement

At the very outset, I would like to thank my advisor, Dr. Prajnaparamita Dhar, Assistant Professor Fred Kurata Memorial Professorship, Department of Chemical and Petroleum Engineering, University of Kansas, for her relentless support and guidance, through thick and thin, without which, it would have been impossible to reach this milestone. I am also grateful to Dr. Laird Forrest, School of Pharmacy, University of Kansas, and Dr. Alan J. Warring, Department of Medicine, University of California Los Angeles, for their generous contributions in the form of nanopartiples (Dr. Forrest) and lung surfactant proteins (Dr. Waring) used in this study. I would also thank my committee members, Dr. Stevin Gehrke and Dr. Kevin Leonard, Chemical & Petroleum Engineering, University of Kansas, for their kind guidance. I would take this opportunity to thank every Professor and staff in the Department of Chemical & Petroleum Engineering, University of Kansas, for providing me with the appropriate ambience. I am also thankful to all my colleagues, especially, Nabil Alhakamy, for their constant encouragement. I gratefully acknowledge Dr. Prem Thapa at the University of Kansas Microscopy and Analytical Imaging facility for obtaining the TEM images. I acknowledge the Bioengineering Research Center (BERC) for access to their AFM. I also acknowledge Mr. Jeff Curley in the Department of Chemical and Petroleum Engineering's machinist for helping us built the stand for inverse Langmuir –Schaffer trough. Last, but by no means the least, I would like to thank my parents, Dr. Nibedita Chakrabarti, Principal, Victoria Institution College, Kolkata- India, and Dr. Manoj Kumar Chakrabarti, Director-in-Charge, NICED (ICMR- Govt. of India), Kolkata- India, for loving me selflessly and showing me the path. I owe every success to them.

Table of Contents

Chapter 1: Introduction……1

1.1 Introduction……2

1.2 Reference……6

Chapter 2: Phospholipid Composition Modulates Carbon Nanodiamond Induced Alterations in Phospholipid Domain Formation……8

2.1 ABSTRACT……9

2.2 Introduction……10

2.3 Materials and Methods……14

2.3.1 Materials……14

2.3.2 Methods……14

2.4 Theory……17

2.4.1 Compressibility Modulus……17

2.4.2 Calculation of line tension changes from domain size distribution……17

2.4.3 Image Analysis……19

2.4.4 Atomic Force Microscopy (AFM)……20

2.5 Results……21

2.5.1 Isotherms……21

2.5.1.1 Isotherms of DPPC……..21

2.5.1.2 Isotherms of DPPG……21

2.5.1.3 Isotherms of DPPC:DPPG……..22

2.5.1.4 Isotherms of DPPC:POPC……..22

2.5.1.5 Isotherms of DPPC:POPG……..22

2.5.2 Compressibility Modulus……23

2.5.3: Fluorescence Images……24

2.5.3.1 Fluorescence Images of DPPC monolayers incubated with ECNs……24

2.5.3.2 Fluorescence Images of DPPG monolayers incubated with ECNs……24

2.5.3.3 Fluorescence Images of DPPC: DPPG monolayers incubated with ECNs…24

2.5.3.4 Fluorescence Images of DPPC: POPC monolayers incubated with ECNs…25

2.5.3.5 Fluorescence Images of DPPC: POPG monolayers incubated with ECNs…25

2.5.4 AFM Images of DPPC: DPPG and DPPC: POPG monolayers incubated with ECNs…..26

2.6 Discussion……27

2.6.1 Effect of lipid headgroup charge on lipid/ECN interactions in pure lipid systems….28

2.6.2 Effect of lipid headgroup charge and membrane packing on lipid/ECN interactions

In mixed lipid systems……30

2.7 Conclusion……31

2.8 FIGURES……32

2.9 References……46

Chapter 3: Synthetic Protein, MiniB, Counters the Effect of Cholesterol in a Simple Binary Mixture of Lung Surfactant Phospholipids at the Air-Water Interface……48

3.1 Abstract……49

3.2 Introduction……49

3.3 Materials and Methods……53

3.3.1 Materials……53

3.3.2 Methods……53

3.4 Theory……55

3.4.1 Compressibility modulus……55

3.4.2 Condensed Area Fraction……55

3.4.3 Determining line tension from domain size distribution……56

3.5 Results……56

3.5.1 Isotherms……56

3.5.2 Compressibility Modulus……58

3.5.3 Flourescence Images……59

3.5.3.1 Phospholipid monolayer domain morphology……60

3.5.3.2 Collapse……61

3.5.4 Percentage Condensed Region……62

3.5.5 Line Tension……62

3.6 Discussion……63

3.6.1 Effect on Mechanical Properties……64

3.6.2 Tug of war: Effect on Lipid Domain Formation……65

3.6.3 Effect on Line Tension……..66

3.7 Conclusion……67

3.8 Figures……68

3.9 References……74

Summary……78

Conclusion and Future Directions……79

List of Figures and Tables

Figures

Figure 1.1: A simplified diagram of the alveoli showing the aqueous interface which contains the lung surfactants [adapted from ref. 4]. (Please note that the surfactant contains other lipids along with proteins)……2

Fig 1.2: Phospholipids, DPPC, DPPG, POPC and POPG, which were used in the study……4

Figure 1.3: A) Hypothesized structure of SPB. The green lines show the disulphide links which stabilizes the dimers. B) SPB holds the squeezed out lipids close to the monolayer during compression preventing material loss……5

Figure 2.1: Surface Pressure vs. mean molecular area isotherms for (A) a DPPC (B) DPPG (C) DPPC:DPPG (75:25) (D) DPPC:POPC (7:3) (E) DPPC:POPG (7:3) monolayers containing 1 wt % (10 μg/ml) ECN……32

Figure 2.2: Compressibility Modulus vs. mean molecular area isotherms for (A) a DPPC (B) DPPG (C) DPPC:DPPG (75:25) (D) DPPC:POPC (7:3) (E) DPPC:POPG (7:3) monolayers containing 1 wt % (10 µg/ml) ECN……33

Figure 2.3: Fluorescence Microscopy images of pure (A) DPPC and (B) DPPG monolayers before (Control) and after adding 1 wt % (10 µg/ml) ECN, at two representative surface pressures. Contrast in these images is due to the selective segregation of bulky phospholipid modified dye molecules into the more fluid regions. The kidney bean structures, characteristic of a pure DPPC system, underwent drastic transitions to more spiral shape due to interactions with the ECNs. The scale bar is 10µm……34

Figure 2.4: Fluorescence Microscopy images of a mixed DPPC:DPPG (75:25) monolayer with a net anionic charge before (Control) and after adding 1 wt % (10 µg/ml) of anionic ECNs. A decrease in the domain size, and increase in number density was noted (Fig 2.13), but unlike a pure DPPC film, no change in the shape of the domains was observed. The scale bar is 10 µm……35

Figure 2.5: Analysis of domain size distribution of DPPC:DPPG and DPPC:POPG monolayers in the absence (A,C) and presence (B,D) of ECNs. The red curve shows the fit to Equation 4 in the main text. The curve fitting yielded an average adjusted R-Squared value of 0.87, indicating the good quality of the fit. The fitting parameters are also shown……36

Figure 2.6: Fluorescence Microscopy images of a mixed (A) DPPC:POPC (7:3) monolayer with a net neutral charge and (B) DPPC:POPG (7:3) monolayer with a net anionic charge and unsaturated lipids before (Control) and after adding 1 wt % (10 µg/ml) of anionic ECNs. The scale bar is 10 µm……37

Figure 2.7: Change in the condensed area fraction with the addition of ECN as a function of surface pressure. Positive values indicate a lowering in the area of the condensed region whereas a negative value

refers to an increase in the area. (A) For DPPC, there was an increase in the domain area with the introduction of ECN and the change decreased sharply with the increase in surface pressure. (B) In case of DPPG, the condensed area fraction reduced as the negatively charged domains repelled the nanoparticles. A similar trend was observed for DPPC:DPPG. For DPPC:POPC, we recorded the highest reduction in area, but the change decreased with an increase in the surface pressure. Finally, we found very little change in the area for DPPC:POPG……..38

Figure 2.8: Changes in the line tension of (A) DPPC:DPPG and (B) DPPC:POPG at two different surface pressures in the absence and presence of 1 wt % (10 µg/ml) of ECN……..38

Figure 2.9: AFM images of the net anionic binary mixtures of phospholipid films transferred onto a solid mica substrate. (A, B): DPPC:DPPG films in the absence and presence of ECN respectively (C,D): DPPC:POPG films in the absence and presence of ECN respectively. (E,F) Show the height analysis of the raised features indicated by white lines in B and D……..39

Figure 2.10: Surface Pressure vs. area per molecule isotherms of (A) DPPC (B) DPPG (C) DPPC: DPPG (75:25) (D) DPPC:POPC (7:3) (E) DPPC:POPG (7:3) monolayers obtained after one hour of incubation with 1 wt % (10 µg/ml) and 10 wt% (100µg/ml) ECN……..40

Figure 2.11: Compressibility Modulus vs. area per molecule isotherms for (A) DPPC (B) DPPG (C) DPPC: DPPG (75:25) (D) DPPC:POPC (7:3) (E) DPPC:POPG (7:3) monolayers obtained after one hour of incubation with 1 wt % (10 mg/ml) and 10 wt% (100µg/ml) ECN……..41

Figure 2.12: Comparison of ECN induced alterations in lipid domains as a result of exposure to different concentrations of ECN (A) DPPG (B) DPPC:POPG mixture……..42

Figure 2.13: TEM images of the ECNs originally suspended in water (A and B) and organic solvent (C and D) show that the ECNs have a tendency to aggregate into sub micron particle size in media, even though

they are about 5-10 nm in the dry powder state. The aggregates show these individual particles in higher resolution images (B and D). Scale: A: 100 nm, B, D: 10 nm, C: 500 nm……..43

Figure 2.14: (A) Fluorescence images of DPPC:POPG films without and with ECN spread on a PBS buffer sub-phase at two representative surface pressures. (B) Line tension analysis from the domain size distributions in (A) show a significant decrease in the line tension in the presence of ECNs……44

Fig 2.15: Detailed height analysis within a condensed domain shows that unlike the significant height change in the LE phase, the raised features within the LC domain do not correspond to ECN aggregates of size ~ 250 nm, since the height of these features is significantly lower than that expected for ECN aggregates that contain carbon nanodiamonds of diameter 5-10 nm……..45

Fig 3.1: Structure of cholesterol (adapted from Avanti Polar Lipids)……51

Fig 3.2: Structure of Mini B. The disulphide link between the N-terminal and C-terminal is given in yellow. This image was adapted from ref. 20……...52

Fig 3.3: Surface pressure vs. mean molecular area isotherms for different lung surfactant mixtures. (A) DPPC:POPG (7:3) with 1% and 5% MiniB. (B) DPPC:POPG with 1% and 5% cholesterol. (C) DPPC:POPG with 1% MiniB and varying concentration of cholesterol (D) DPPC:POPG with 5% MiniB and different weightage of cholesterol. The isotherms indicate an improvement in surface tension lowering abilities with 1% of both Mini B and cholesterol in the mixture……...68

Fig 3.4: Compressibility Modulus for different lung surfactant mixtures. (A) DPPC:POPG (7:3) with 1% and 5% MiniB. (B) DPPC:POPG with 1% and 5% cholesterol. (C) DPPC:POPG with fixed MiniB percentage (1%) and varying weightage of cholesterol (D) DPPC:POPG with 5% MiniB and different amounts of cholesterol. Higher concentration of MiniB and cholesterol makes the monolayer more compressible whereas lower

concentration of the increases the compressibility. An increase in compressibility modulus implies more packing and is therefore, favorable.....69

Fig 3.5: Fluorescence images of DPPC:POPG (7:3) along with MiniB and cholesterol in varying concentrations. Images A, B, C, G, H, I, M, N, O, P, Q and R were taken at 20 mN/m which lies in the two-phase coexistence region and the rest were taken at 30 mN/m which marks the upper boundary for the same region. Beyond this point, the domains get highly packed for the control. The first two rows are for samples without MiniB, the next couple rows are for samples with 1% MiniB in them, and the last two are for ones with 5% MiniB. Concentration of cholesterol increases from left to right. The images reveal the inherent tendency of cholesterol to stretch out domains whereas, the MiniB showed opposite characteristics.....70

Fig 3.6: Fluoresecence images of DPPC:POPG(7:3) with different concentrations of MiniB and cholesterol after collapse. Concentration of MiniB changes columnwise whereas, the concentration of cholesterol changes along a row. MiniB produces thick cracks (D and G) upon collapse but cholesterol collapses irreversibly (B and C). With both put together, cracks can still be observed in case of 1% MiniB with 1% cholesterol (E) or 5% MiniB with 1% cholesterol (H). However, cholesterol dominates at higher concentration (F and I). DPPC:POPG on its own produces thin collapse cracks (A).....71

Fig 3.7: Percentage condensed domains for varying mixtures of DPPC:POPG (7:3). Percentage condensed domains show the amount of area that has condensed in the two-phase coexistence region. (A) Effect of MiniB on DPPC:POPG has been shown here. A reduction in the area was noted for 5% MiniB. (B) cholesterol reduces the area and the effect is more pronounced with an increase in choleserol concentration. (C) Interaction of 1% MiniB with different concentrations of cholesterol has been shown in this graph. Interestingly, 1% MiniB along with 1% cholesterol (inverted triangle) increases the area of the condensed domains. (D) 5% MiniB along with different concentrations of cholesterol showed decrease in area everytime.....72

Fig 3.8: Changes in line tension for different mixtures. (A) MiniB increases the line tension between the domains (B) We could only measure the line tension for 5% MiniB with 1% cholesterol and 5% MiniB with 5% cholesterol as these domains were circular in shape. 1% MiniB with 1% cholesterol did not lower the line tension whereas, 5% of both revealed a lowering in line tension……..73

Tables

Table 2.1: List of phospholipid combinations studied along with their overall charge and saturation…….13

Table 2.2: Particle size analysis of the ECNs in different media relevant to the experimental conditions…16

Table 3.1: The table summarizes the LS mixtures tested in this study. Numbers refer to the amount by weight of MiniB and cholesterol that was added to a mixture of DPPC: POPG (7:3)……54

Chapter 1

Introduction

1.1 Introduction

Lung surfactants [LS] are a complex mixture of lipids and proteins that are present in the alveolar lining of the lungs [1]. The primary function of LS is to lower surface tension to near zero mN/m with expiration [2]. This is of utmost importance as a large pressure is needed to ventilate the lungs and therefore, in the absence of lung surfactants, smaller alveoli would collapse to larger ones, leading to uneven ventilation and the lungs would eventually collapse. LS essentially reduce the energy involved in breathing as lesser pressure is needed to inflate smaller alveoli. The smaller alveoli in turn, ensure a large surface area which enables greater gas exchange. These, along with the other functions, have been elaborately presented by Frerking et. al [3]. Fig1.1 shows a simplified diagram of alveoli [4]. The monolayer of lung surfactant lipids form at the air-water interface. Apart from lowering surface tension, LS can also play a role in immune response [5]. Any foreign particle that can enter lungs, interacts with LS. Thus, nanoparticles that can be used for the purpose of drug delivery, can encounter these surfactants and interact either favorably or adversely; a topic that will be covered in greater details in chapter 3.

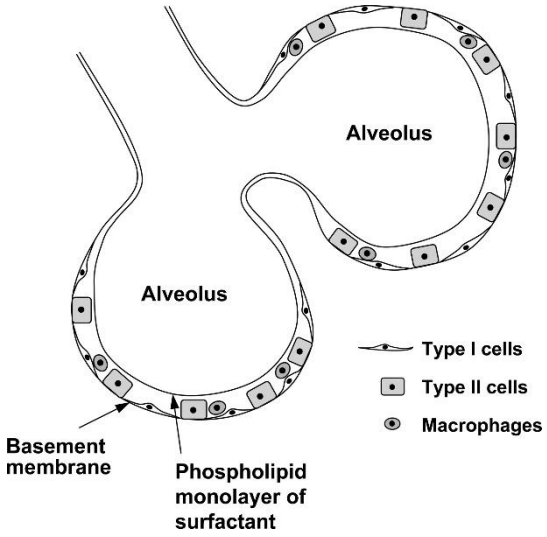

Figure 1.1: A simplified diagram of the alveoli showing the aqueous interface which contains the lung surfactants [adapted from ref. 4]. (Please note that the surfactant contains other lipids along with proteins).

Naturally, an absence or dysfunction of LS is a cause of concern as it may become fatal. Many infants born premature, fail to produce LS on their own, which leads to Neonatal Respiratory Distress Syndrome [NRDS] [6]. In USA itself, a high percentage of low weight infants are diagnosed with NRDS (around 70% during the 90s) and across the world, NRDS contributes to about 40% of the mortality of children younger than 5 years [7]. A dysfunction in LS has also been reported to be associated with Acute Respiratory Distress Syndrome [ARDS]/ Acute Lung Injury [ALI] and each year, around 50,000-190,000 such cases are reported in USA [8]. Medical intervention in the form of Surfactant Replacement Therapy [SRT] is needed to take measures against such diseases and thus, great attention has been put into understanding the composition of LS and the interaction between the different components.

LS is composed of around 80% phospholipids [9]. The primary component of the phospholipids is 1,2-dipalmitoyl-*sn*-glycero-3-phosphocholine (DPPC). DPPC is a zwitterionic lipid with two saturated, hydrophobic chains of palmitic acid. The saturated chains allow the monolayers of the surfactants at the air-water interface of the alveoli to compress to very low values of surface tension before the film collapses. This is possible as the saturated chains can assemble to highly ordered state of existence. Thus, these saturated lipids play a crucial part in lowering surface tension in the lungs. Although the saturated lipids can efficiently lower surface tension, they fail to get adsorbed quickly to the surface. Quick adsorption to the surface is much needed in order to prevent any delay in the process of breathing. Thus, LS also comprises of unsaturated lipids that cannot assemble to a highly packed form. However, they can be easily adsorbed to the surface and also help the LS to spread rapidly. These features are vital and make the compositions of the LS dynamic. The head-groups of the phospholipids are hydrophilic and remain soluble in the aqueous lining of the alveoli. Around 85% of the phospholipids are Phosphatidylcholine (PC) which is zwitterionic. About 9% of the phospholipids are Phosphatidylglycerol (PG) which has a net negative charge. A minute quantity of zwitterionic, Phosphatidylethanolamine (PE, 3%) and negatively charged phosphatidylinositol (PI, 2%) are also present in LS. Other than the phospholipids, around 10% of

the surfactants contain neutral lipids, primarily cholesterol, and some amount of free fatty acids and triglycerides. Cholesterol plays a part in improving the fluidity of the lung surfactant mixture and will be discussed in depth in chapter 2 where the interaction of cholesterol with an artificial surfactant protein called Mini B has been studied. The structures of the lipids used in the study are shown in Fig 1.2.

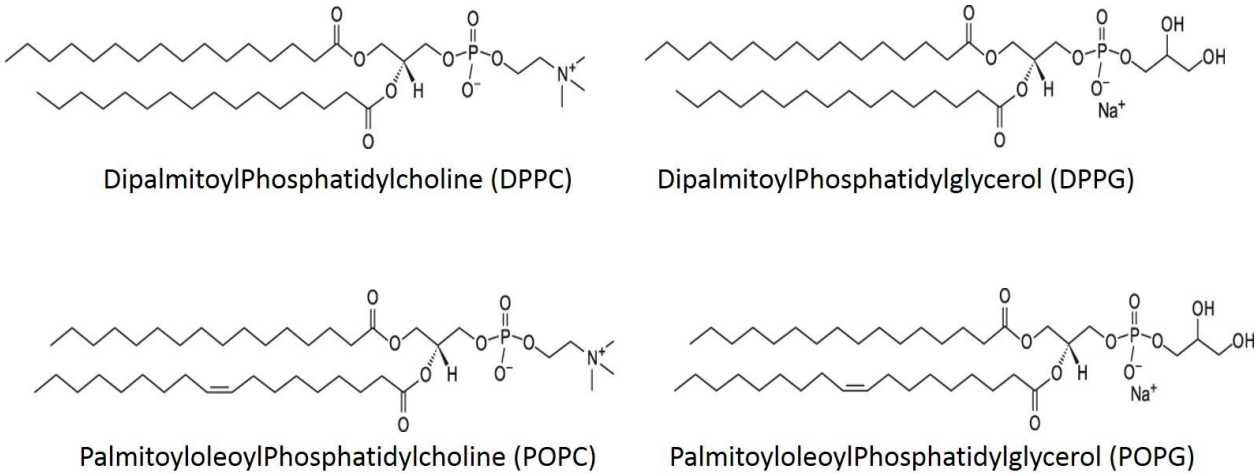

Figure 1.2: Phospholipids, DPPC, DPPG, POPC and POPG, which were used in the study. The structures were adapted from Avanti Polar Lipids, inc.

The remaining 10% of the surfactants are the proteins, namely SPA, SPB, SPC and SPD [9]. Among these, SPA and SPD are hydrophilic proteins [9]. SPA plays a part in homeostasis as well as surfactant turnover. The functions of SPA and SPD were discussed in details by Kishore et. al. [10] and both these large proteins are involved in immune response. On the other hand, SPB and SPC are hydrophobic in nature and help in forming and maintaining the surfactant films at the air-water interface [11]. Even though the exact 3D structure of SPB is unknown, studies have shown that it is mainly alpha helical (40-45%) with 79 amino acids. In a monolayer containing LS phospholipids, SPB attaches itself to the liquid-expanded region making the condensed domains smaller in size but greater in number which gives stability to the cell. SPB is also charged, having 9 positively amino acid residues, which is believed to interact with the anionic

headgroup of the phospholipids [12]. We are particularly interested in SPB, because Mini B, the synthetic protein that we have studied, is an analog of the naturally occurring surfactant protein SPB. Fig 1.3 shows the hypothesized structure of SPB based on data from the indirect techniques, such as Circular Dichroism, Spin-resonance, infrared spectroscopy and Fluorescence anisotropy. During compression of the monolayer, as we breathe out, unsaturated lipids squeeze out of the surface and SPB is believed to interact with them, holding them close to the surface which has been shown in Fig 1.3 B.

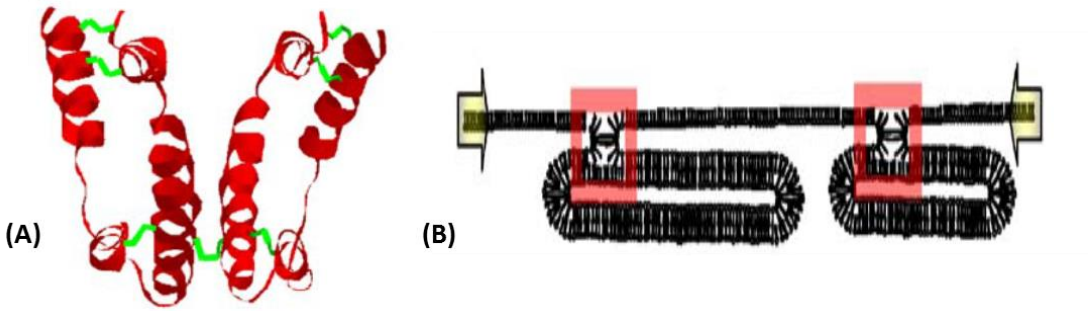

Figure 1.3: A) Hypothesized structure of SPB. The green lines show the disulphide links which stabilizes the dimers. B) SPB holds the squeezed out lipids close to the monolayer during compression preventing material loss. [Adapted from ref. 12]

In Chapter 2 we discuss the results of our study focused on understanding the role of phospholipid composition in modulating phospholipid interactions with a model nanoparticle system with wide biomedical applications, namely, Engineered Carbon Nanodiamonds [ECN]. In chapter 3 we describe our assessment of the role of a synthetic lung surfactant protein called Mini B in countering the adverse effects of cholesterol, which is a highly debatable component in Surfactant Replacement Therapy [SRT].

1.2 References

1. Saxena, S., *Lung surfactant.* Resonance, 2005. **10**(8): p. 91-96.
2. Zhang, H., et al., *On the Low Surface Tension of Lung Surfactant.* Langmuir, 2011. **27**(13): p. 8351-8358.
3. Frerking, I., et al., *Pulmonary surfactant: functions, abnormalities and therapeutic options.* Intensive Care Medicine, 2001. **27**(11): p. 1699-1717.
4. Andreeva, A.V., et al., *Regulation of Surfactant Secretion in Alveolar Type II cells.* American journal of physiology- Lung cellular and Molecular Physiology, 2007. **293**(2): p. L259-L271.
5. Wright, J.R., *The "wisdom" of lung surfactant: balancing host defense and surface tension-reducing functions.* American Journal of Physiology - Lung Cellular and Molecular Physiology, 2006. **291**(5): p. L847-L850.
6. Notter, R.H. and D.L. Shapiro, *Lung Surfactant in an Era of Replacement Therapy.* Pediatrics, 1981. **68**(6): p. 781.
7. Kamath, B.D., et al., *Neonatal Mortality From Respiratory Distress Syndrome: Lessons for Low-Resource Countries.* Pediatrics, 2011. **127**(6): p. 1139-1146.
8. Krishnan Raghavendran, D.W., R.H. Notter, *Surfactant Therapy for Acute Lung Injury and Acute Respiratory Distress Syndrome.* Critical Care Clinics, 2011. **27**(3): p. 525-559.
9. Jesús, P.-G., *Molecular Interactions in Pulmonary Surfactant Films.* Biology of the Neonate, 2002. **81**: p. 6-15.
10. Kishore, U., et al., *Surfactant proteins SP-A and SP-D: Structure, function and receptors.* Molecular Immunology, 2006. **43**(9): p. 1293-1315.
11. Weaver, T.E., *Synthesis, processing and secretion of surfactant proteins B and C.* Biochimica et Biophysica Acta (BBA) - Molecular Basis of Disease, 1998. **1408**(2–3): p. 173-179.

12. Serrano, A. G. and Jesús, P.-G., Protein–lipid interactions and surface activity in the pulmonary surfactant system. Chemistry and physics of lipids, 2006. **141**(1-2): p. 105-118.

Chapter 2

Phospholipid Composition Modulates Carbon Nanodiamond-Induced Alterations in Phospholipid Domain Formation*

*Adapted from Chakraborty, A., et al., Phospholipid Composition Modulates Carbon Nanodiamond-Induced Alterations in Phospholipid Domain Formation. Langmuir, 2015 **31**(18): p. 5093- 5104.

2.1 ABSTRACT

The focus of the work described in this chapter is to elucidate how phospholipid composition can modulate lipid nanoparticle interactions in phospholipid monolayer systems. We report on alterations in lipid domain formation induced by anionic engineered carbon nanodiamonds (ECNs), as a function of lipid headgroup charge and alkyl chain saturation. Using surface pressure vs. area isotherms, monolayer compressibility and fluorescence microscopy, we found that anionic ECNs induced domain shape alterations in zwitterionic phosphatidylcholine lipids, irrespective of the lipid alkyl chain saturation, even when the surface pressure vs. area isotherms did not show any significant changes. Bean-shaped structures characteristic of dipalmitoylphosphatidylcholine (DPPC) were converted to multilobed, fractal or spiral domains as a result of exposure to ECNs, indicating that ECNs lower the line tension between domains in case of zwitterionic lipids. For membrane systems containing anionic phospholipids, ECN induced changes in domain packing were related to the electrostatic interactions between the anionic ECNs and the anionic lipid headgroups, even when zwitterionic lipids are in excess. By comparing the measured size distributions with our recently developed theory derived by minimizing the free energy associated with the domain energy and mixing entropy, we found that the change in line tension induced by anionic ECNs is dominated by the charge on the condensed lipid domains. Atomic force microscopy images of the transferred anionic films confirm that the location of the anionic ECNs in the lipid monolayers is also modulated by the charge on the condensed lipid domains. Since biological membranes such as lung surfactants, contain both saturated and unsaturated phospholipids with different lipid headgroup charges, our results suggest that when studying potential adverse effects of nanoparticles on biological systems, the role of lipid compositions cannot be neglected.

2.2 Introduction:

Recent advances in the field of nanotechnology have led to increased use of engineered nanoparticles (ENPs) in commercial applications such as electronic components, cosmetics, surface coatings, scratch-free paints, as well as biomedical applications such as targeted drug delivery [1, 2]. The small size of these engineered nanoparticles leads to altered chemical reactivity when compared with their bulk counterparts. Additionally, their extremely small size makes ENPs increasingly capable of entering the human body either through environmental exposure or intentionally by inhalation, ingestion, skin penetration or being directly injected as in the case of several medical applications. While their altered chemical reactivity and small size make ENPs desirable for multiple commercial and medical applications, their potential toxic impact on biological materials, living organisms, and the environment is not yet well understood and is therefore a cause for concern [3].

The respiratory route represents a unique portal of entry for inhaled nanoparticles, resulting in their accumulation in the lung. It has long been known that nanoparticles with hydrodynamic radius 10-20 nm are predominantly deposited in the alveolar regions, where they are expected to interact with lung surfactants (LS), a mixture of lipids and proteins that are together responsible for maintaining a low surface tension in the lung and prevent collapse [4-6]. However, analysis of the nanoparticle deposition has also shown that these smaller nanoparticles are often exhaled out during expiration. Rather, nanoparticles and nanoparticle agglomerates of size ranges 0.1-2 μm are more likely to be retained in the alveolar regions [7, 8]. As a result, the last few years have seen an increase in studies focused on the biophysical interactions of LS with polymeric and metallic nanoparticles of different composition, size, surface potential, or modified surface chemistry. Unfortunately, many of these studies have demonstrated contradictory effects of the nanoparticles on LS, as summarized below.

Galla and co-workers, have reported concentration dependent adverse effects of hydrophobic polyorganosiloxane (AmOrSil20) on the surface tension lowering ability of a model LS. They observed an

increased fluidization of the phospholipid monolayers due to interaction with the hydrophobic nanoparticles [9]. In a follow-up article, this group used high resolution microscopy imaging to further show that the AmOrSil20 nanoparticles influence the insertion of surfactant vesicles into the air/lipid interface in a concentration dependent manner, possibly by associating with surfactant associated reservoirs of LS at higher nanoparticle concentrations and surfactant packing [10], while associating with fluid regions of the film at lower surface pressures. More recently, these authors have also provided evidence of molecular rearrangement of model LS around these hydrophobic nanoparticles [11], which may also be effected by the size of the hydrophobic nanoparticles [12]. Similarly, Zuo and coworkers have not only demonstrated time dependent adverse effects of hydroxyapatite nanoparticles on surfactant vesicles of a clinical surfactant Infasurf [13], but also demonstrated a difference in their translocation propensity through lipid monolayers [14]. In contrast, Beck-Broichsitter et al. reported that polystyrene nanoparticles of size 100 nm demonstrated no change in the surface tension lowering ability of another clinical surfactant (Alveofact) at a range of different concentrations [15]. Further, Farnoud et al. showed that 200 nm sized carboxyl modified polystyrene particles had opposite effects on the packing of dipalmitoylphosphatidylcholine (DPPC) films depending on their mode of exposure. When nanoparticles were injected below a preformed DPPC film, no penetration of the nanoparticles was noted. However, when the phospholipid was spread on a nanoparticle laden sub-phase, significant alteration of the DPPC packing was observed. The authors suggest that the sequence of particle and monolayer addition may influence nanoparticle−lipid interactions [16].

Adverse effects of metallic nanoparticle-lung surfactant lipid interactions on the surface tension lowering ability was reported for TiO_2 nanoparticles of size ~5 nm, but not for microparticles of TiO_2 [17, 18], suggesting that the size of these metallic nanoparticles contribute to their interactions with lipids. Along similar lines, Kodama et al., recently presented evidence of existence of a critical particle size range that effects the phospholipid domain packing of a model lung surfactant [19]. Bakshi et al. reported that bare

gold nanoparticles of size 15 nm impeded the ability of model lung surfactants to lower the surface tension [20], and led to aggregation of surfactant protein SP-B, preventing efficient adsorption of surfactant to the air/water interface. Contrary to these results, Tatur and Badia demonstrated a contrasting behavior in case of pure or mixed phospholipid monolayers exposed to hydrophobic alkylated gold nanoparticles of average core diameter 2 nm [21]. Their results indicated that even though these functionalized gold nanoparticles did not alter the surface tension lowering ability of lung surfactants, they altered the shape and size of liquid-condensed domains in DPPC films, that was used as a model protein-free LS. Interestingly, no adverse effects were seen for a clinical surfactant, Survanta [21] (containing both saturated and unsaturated lipids as well as surfactant proteins) even at nanoparticle concentrations that were two orders of magnitude higher than in the case of exposure to DPPC. These results suggested that the composition of lipid monolayers, and association of gold nanoparticles with the lipid domains played a dominant role.

The contrasting results of the effect of nanoparticles on phospholipid packing in model lung surfactant function and particularly, the potential role of surfactant composition on lipid nanoparticle interactions form the major motivations for this study. While the effect of the shape, size and surface chemistry of the nanoparticles themselves have been studied in detail, to the best of our knowledge the effect of lipid headgroup charge and lipid saturation on nanoparticle induced changes in lipid domain formation and lipid packing is currently unknown. Therefore, the focus of this work is to understand how differences in lipid composition alter their interactions with nanoparticles. In particular, we report on the alterations in lipid domain packing of five different lipid compositions with different alkyl chain saturation and headgroup charge (Table 2.1) induced by surface modified engineered carbon nanodiamonds (ECNs) with a net negative charge.The choice of lipids is explained in detail in the discussion section and aims to reflect the major phospholipid headgroups (phosphatidylcholine, PC and phosphatidylglycerol, PG) in native and synthetic LS mixtures. Since both saturated and unsaturated lipids are essential for proper functioning of

LS, our choice of lipid compositions also reflects the alkyl chain saturations present in LS. ECNs were picked as our choice of nanoparticles since they have recently received a lot of attention due to their potential applications in drug delivery, biomedical imaging and tissue engineering applications [22] and are regularly used by co-author Forrest for *in vivo* applications [23, 24]. Therefore, understanding the fundamental physical rules governing lipid-nanapoarticle interactions using these nanoparticles are significant from a nanotoxicity perspective.

Table 2.1: List of phospholipid combinations studied along with their overall charge and saturation.

Sample	Saturated	Net charge
DPPC	Yes	Neutral
DPPG	Yes	Anionic
DPPC:DPPG (75:25)	Yes	Anionic
DPPC:POPC (7:3)	No	Neutral
DPPC:POPG (7:3)	No	Anionic

2.3 Materials and Methods:

2.3.1 Materials: Phospholipids dipalmitoylphosphatidylcholine (DPPC), dipalmitoyl phosphatidylglycerol (DPPG), 1-palmitoyl-2-oleoyl-*sn*-glycero-3-phosphocholine (POPC) and 1-palmitoyl-2-oleoyl-*sn*-glycero-3-phospho-(1'-*rac*-glycerol) (POPG) used in this study were purchased from Avanti Polar Lipids (Alabaster, AL) as organic mixtures in chloroform at a final concentration of 5 or 25 mg/ml. Texas Red® 1,2-dihexadecanoyl-*sn*-glycero-3-phosphoethanolamine, triethylammonium salt, TXR-DHPE, lipid dye was purchased in the dried form from Life Technologies (Invitrogen, Grand island, NY) and dissolved in high performance liquid chromatography (HPLC) grade chloroform (final concentration of 0.5 mg/ml). All organic solvents used for this work were purchased from Thermo Fisher Scientific Inc. (Pittsburgh, PA). The sub-phase water (resistivity 18.2 MΩ/cm) was prepared using a Millipore Gradient System (Billerica, MA). The lipid mixtures were stored at -20 ˚C when not in use to ensure no evaporation of the organic solvent. The carbon nanodiamonds used in this study were obtained from Microdiamant, Lengwil, Switzerland.

2.3.2 Methods: Stock solutions of pure DPPC or DPPG, or mixed phospholipids of DPPC:DPPG, DPPC:POPC, DPPC:POPG in the ratio 70:30 molar ratio for DPPC:POPC and DPPC:POPG and 75:25 molar ratio for DPPC:DPPG were mixed with 0.5 mol % of TXR-DHPE dye in HPLC grade chloroform:methanol (4:1) mixtures. The ratio of 7:3 was selected primarily because many synthetic lung surfactant mixtures contain this ratio of PG. Stock solutions of the ECN were prepared by suspending the ECNs initially in water and in the methanol chloroform mixture and allowing the solution to sonicate for two hours. Immediately at the end of the sonication process, the particle size and zeta potential (for the aqueous sample) of the samples was measured using dynamic light scattering (NanoBrook Omni, from Brookhaven Instruments Corporation). The particle size was also measured in the presence of phospholipids in the organic solution. For these samples, stoichiometric volumes of the ECN were added to the organic lipid solution immediately after sonication, and used for particle size analysis or for the Langmuir trough experiments

described below. Table 2.2 shows the particle size distribution, obtained using the Smoluchowski equation that is built into the software. Our results showed that the carbon nanodiamonds formed aggregates of effective size 219 nm (average of three measurements), with a polydispersity of 0.19 when dispersed in water while the effective size of the aggregates in the organic mixture used for further experiments was found to be 235 nm with a a polydispersity of 0.35 . Further, we found that this aggregate size did not change within the first half hour after sonication, ensuring that the particle size did not change during the experiment. The zeta potential was measured using a 1.0 mM KCl solution, and was found to be -28 mV. The anionic nature of the ECN surface is a result of the interactions of these nanodiamond powders with air or ozone (during the purification process), which typically results in the presence of COOH groups on the ECN surface [22]. This anionic nature of the ECNs enables several surface modifications that are advantageous for various delivery-based applications [22].

To initiate each experiment on the Langmuir trough, the lipid/nanoparticle mixture was made in chloroform:methanol mixture (4:1) and was added drop-wise from a Hamilton glass syringe onto a water sub-phase equilibrated to a temperature of 22 $^{\circ}$C at a pH of 5.6, contained in a ribbon Langmuir trough (Biolin Scientific Inc.) of maximum area 166 cm^2 and minimum area 46 cm^2. In these experiments, water was chosen as the sub-phase of choice to eliminate the effect of cations on the phospholipid packing, and to compare and contrast our results with previous biophysical measurements using similar phospholipid systems where water was chosen as the sub-phase [9, 21, 25, 26]. The moveable ribbon allowed controlled compression and expansion of the lipid monolayer formed at the interface, serving as an *in vitro* model mimicking change in alveoli area during inhalation and exhalation. Only the compression cycle is shown here. The trough is computer controlled using the trough control software from at Biolin Scientific. After spreading the sample, the solvent was allowed to evaporate by waiting for 20 minutes before any compression was started. In this study the monolayer compression rate was kept at 7.0 cm^2/minute. This rate is slow enough to allow time for simultaneous focusing on the monolayer film during compression

and also mimic a quasi-static compression rate. Compression studies were also conducted at 125 cm^2/minute, to ensure that the changes in the isotherms were not dependent on the rate of compression. A wet calibrated filter paper was used as a Wilhelmy plate balance allowing continuous recording of the surface pressure during the compression/expansion cycles. The Langmuir trough was mounted on a custom modified Nikon Eclipse fluorescence microscope with motorized focusing to allow continuous monitoring of the surface morphology during film compression. A 40x long working distance objective designed for fluorescent light was used to view the lipid monolayer film. A dichroic mirror/barrier filter assembly directed the excitation light onto the monolayer films at a normal angle of incidence and filtered the emitted light. The images were detected by a fast CCD camera (Andor LUCA) and short image sequences (5 frames) were recorded at every 1-5 mN/m surface pressure interval depending on the sample and the surface pressures.

Table 2.2: Particle size analysis of the ECNs in different media relevant to the experimental conditions.

ECN in	Particle Size (nm)	Poly-dispersity
Water	219	0.19
Chloroform/ methanol mixture	240	0.35
Lipid/organic mixture	130	0.41

2.4 Theory:

2.4.1 Compressibility Modulus: The compressibility of a lipid monolayer is sometimes used to describe monolayer mechanical properties. The isothermal two-dimensional bulk modulus of a material can be described as the material's ability to store mechanical energy as stress. Mathematically, this two-dimensional bulk modulus, β is defined as:

$$\beta = -A\left(\frac{\partial \Pi}{\partial A}\right)_T = A\left(\frac{\partial \gamma}{\partial A}\right)_T = 1/\kappa \qquad (1).$$

The inverse of β is defined as the isothermal compressibility, κ, and is often used to quantify mechanical properties of lipid monolayers. Note that β and κ are both 2nd order derivatives of the free energy, *G.* $\gamma = \left(\partial G/\partial A\right)_T, \beta = \left(\partial^2 G/\partial A^2\right)_T$ Therefore a dip in an experimentally obtained vs. A profile (or a discontinuous change at which $\beta \to 0$ or $\kappa \to \infty$) signifies a first order phase transition. In addition, a higher incompressibility suggests the formation of condensed well-packed films, and is essential for proper functioning of LS. For our experimental results, the compressibility modulus was calculated by taking the derivative of the surface pressure vs. area isotherms using in-built functions in Origin 8.62. The data was smoothened using a FFT filter over 5 points for all points except near the monolayer collapse region.

2.4.2 Calculation of line tension changes from domain size distribution: It is now well-known that lipid molecules at the interface undergo lateral organization of the molecules to form domains [27]. Theoretical and experimental work by McConnell and co-workers have shown that distribution of domain sizes and shape in monolayers is a result of a balance between the interfacial energy at the domain edges (line tension) and electrostatic interactions between domains [28-30]. The difference in lipid chain lengths between the liquid-ordered (l_o) and liquid-disordered (l_d) phases (or liquid condensed (LC) and liquid

expanded (LE) phases in case of monolayers) leads to a line tension, λ, proportional to the hydrophobic mismatch between domains and the interfacial tension of the hydrocarbon-air interface ($\lambda \propto (l_o - l_d)\gamma$). Similarly, a difference in the packing density and composition between lipid phases results in a change in the average dipole density ($\Delta m^2 = m_o - m_d$) due to electrostatic repulsion between and within the domains. This electrostatic repulsion in turn leads to changes in the electrostatic energy of the film. However, these parameters are often difficult to measure, particularly in the presence of small impurities, such as the ECN in this work. We have previously demonstrated a technique to calculate the line tension and dipole density difference of phospholipid domains by comparing the measured size distributions with a theory derived by minimizing the free energy associated with the domain energy and mixing entropy [31, 32]. In these systems we assume that the domains are in equilibrium. Briefly, for a circular domain, the radius of the domain (R) is related to the energy *E* by the equation:

$$\frac{E}{N} = \frac{2a_0}{R}\left[\lambda - \frac{\Delta m^2}{4\pi\varepsilon\varepsilon_o}\ln\left(\frac{4R}{e^2\Delta}\right)\right] \qquad (2)$$

In this expression, line tension, λ, between the domains of area a_0 promotes fewer, larger domains, and the dipole density difference, Δm^2, (C/m) between the domains, promotes smaller, more numerous domains, Δ is a length on the order of molecular dimensions, ~ 1 nm, ε is the dielectric constant of water (~80) and ε_o, the permittivity of free space (= 8.854 x 10^{-12} C^2/J-m) [28]. N is the number of molecules with radius R, and can be given by minimizing equation 2 shows that minimum energy radius, R_o, for an isolated domain is:

$$R_0 = \frac{e^3\Delta}{4}[\exp(\frac{4\pi\varepsilon\varepsilon_0}{\Delta m^2}\lambda)] \qquad (3)$$

However, our results demonstrate that the lipid domains at interfaces are polydisperse, and do not alter their shapes for several hours. This observation suggests the role of entropy of mixing, leading to a domain

size distribution. Assuming ideal entropy of mixing (i.e. no interactions between domains), and equality of the chemical potential of lipid condensed domains of radius R or R_0, we have shown that one can write an equation for the number fractions of domains ($C_{N,M}$) with *N* (radius *R*) or *M* (radius R_o) molecules, in terms of the radius of the domains of molecules N and M [31]:

$$C_N = [C_M * \exp\{-\frac{\Delta m^2 R_0}{4\varepsilon_0 \varepsilon kT}(R_0/R-1)^2\}]^{R^2/R_0^2} \quad (4)$$

Equation 4 is used to fit the experimentally obtained domain size distributions, using C_M, $\frac{\Delta m^2 R_0}{4\varepsilon_0 \varepsilon kT}$, and R_0, as the three fitting parameters (fits of adjusted r-squared values greater than 0.8 were accepted as good fits). Equation 3 is then used to calculate the line tension.

2.4.3 Image Analysis: All fluorescence microscopy images were analyzed using ImageJ (NIH). To calculate the total change in the packing of the lipid ordered domains, change in the area fraction of the ordered condensed domains (the dark domains in the images) is calculated using the following equation:

$$Change\ in\ Condensed\ Area\ Fraction = \frac{Condensed\ Area\ Fraction\ of\ Control - Condensed\ Area\ Fraction\ with\ ECN}{Condensed\ Area\ Fraction\ of\ Control}$$

where:

$$Condensed\ Area\ Fraction = \frac{Area\ of\ Dark\ Domains}{Total\ Area\ of\ Frame}$$

The domain size distribution is plotted as normalized histograms with the width of the size distribution being set by dividing the maximum measured domain size by the square root of the number of domains analyzed, $n^{1/2}$. The minimum resolved domain radius was set to be 0.5 µm, which was determined by the resolution of the optical microscope.To improve the statistics, two neighboring frames were analyzed. To represent the histogram as a probability distribution, we represent the number of domains as a relative frequency. Using the Nonlinear Curve Fit feature of Origin 8.6, the domain size distribution of DPPC:DPPG

and DPPC:POPG domains with and without ECNs were fit to Equation 4, and the fitting parameters used to calculate the line tension of these monolayers.

2.4.4 Atomic Force Microscopy (AFM): The location of the ECNs in the anionic lipid monolayers inferred from the domain size distribution of DPPC:DPPG and DPPC:POPG domains with and without ECNs were correlated with high resolution AFM images of the phospholipid films at a surface pressure of 20 mN/m transferred onto a freshly cleaved mica substrate . A home-built inverse Langmuir-Schaffer technique similar to the technique developed by Lee et al. was used for the film transfer process [33]. This technique allows visualization of the film during the transfer process, to ensure that there were no perturbations in the domain distribution during the transfer process. Briefly, the mica substrate was placed on an aluminum holder with machined knife-edges following the design of Lee et al [33]. This whole apparatus was first thoroughly cleaned and then placed on the bottom of the trough, and kept submerged during the compression cycle. When the desired surface pressure was reached, the water was very slowly aspirated, until the knife-edge cut the monolayer, and let it fall onto the substrate. The focus was re-adjusted throughout the process to ensure that the surface was always visible.

The transferred monolayers were imaged at the ambient temperature in air using a Veeco diMultimode V microscope. A J-scanner with an X-Y scan range of 125 by 125 μm was used in the tapping mode using Antimony doped Silicon probes (Bruker Scientific) with a resonant frequency of 371 kHz. Images were collected at a scan rate of 1 μm/sec at a resolution of 512 pixels/line. The images were later flattened using the in-built software to compensate for sample tilt (raised features were excluded from this flattening). The captured images were exported and saved for further use and height analysis.

2.5 Results:

2.5.1 Isotherms:

2.5.1.1 Isotherms of DPPC: Figure 2.1A shows a quasi-static surface pressure vs. mean molecular area isotherm for a DPPC film containing 1.0 wt% (10 µg /ml) of ECN. The averages of three sets are plotted. Surface pressure is defined as $\Pi=\gamma_0-\gamma$, where γ_0=72 mN/m for water, and γ is the measured surface tension. The red dashed line shows a characteristic surface pressure vs. mean molecular area of pure DPPC film. At very high area per molecule, the monolayer was in a gas phase, with a nearly zero surface pressure. As the area of the trough was decreased, the total area exposed to the molecules increased, which in turn caused the surface pressure to increase from zero. With increased compression, the film entered the liquid expanded (LE) phase, which was accompanied by a smooth increase in the surface pressure until a plateau was reached at Π= 7mN/m, corresponding to the start of the liquid condensed (LC) region. The presence of a plateau region on further compression of the trough was due to an increase in the fraction of LC domains at the expense of the LE phase at a nearly constant surface pressure (co-existence plateau). At the end of this coexistence plateau, the surface pressure increased almost linearly with decreased molecular area, until the film underwent collapse at a surface pressure ~72 mN/m. The black dashed dot curve shows the measured surface pressure vs. mean molecular area after the DPPC film had been incubated with ECN. No significant changes in the collapse surface pressure or the surface pressure corresponding to LE/LC coexistence plateau were noted when the DPPC solution was incubated with 1.0 wt. % (10 µg /ml) ECN. However, the addition of ECN did cause a shift of the curves to smaller mean molecular areas occupied by the lipid molecules, suggesting that the ECNs have a condensing effect on the DPPC domains.

2.5.1.2 Isotherms of DPPG: Figure 2.1B shows a typical surface pressure vs. mean molecular area isotherm for a DPPG film containing 1.0 wt. % (10µg/ml) of ECN. As expected, based on previous reports, pure DPPG film (red dashed curve) at room temperature did not show an explicit LE/LC coexistence plateau seen for

DPPC. Vollhardt et al. showed that this is because DPPG films on a pure water sub-phase already existed as a LC phase at surface pressure of 0 mN/m [34]. Upon compression, the surface pressure increased sharply until the film underwent monolayer collapse at a surface pressure of around 60 mN/m. Adding 1.0 wt. % (10 μg/ml) ECN did not alter this surface pressure vs. area isotherm.

2.5.1.3 Isotherms of DPPC:DPPG: DPPC:DPPG was used as a model lipid system containing a net negative charge due to the PG headgroup, while the alkyl tail length and tail saturation was the same for both the lipids. This model mixture has previously been used by Harishchandra et al. to study the effect of hydrophobic AmOrSil20 on model lipid films. As seen in Figure 2.1C, the characteristic surface pressure vs. mean molecular area isotherm (red dashed curve) resembled that of a pure DPPG film, with no LE/LC coexistence region typical of a DPPC film, but had a collapse surface pressure corresponding to a DPPC film. No changes in the pressure area isotherms were observed when 1 wt % (10 μg/ml) of ECN was added to this lipid mixture (black dash dot line).

2.5.1.4 Isotherms of DPPC:POPC: Introduction of unsaturated POPC molecules with mixed alkyl chains alters the ability of DPPC molecules to form well-packed structures. As a result, the addition of POPC significantly alters the surface pressure vs. mean molecular area isotherms compared to a characteristic DPPC film. As shown in the red dashed curve in Figure 2.1D, the LE/LC coexistence plateau was not present at surface pressure ~7 - 9 mN/m; however, a shoulder appeared at a surface pressure of ~42 mN/m, corresponding to the collapse pressure of pure POPC films. This shoulder corresponds to the "squeeze-out" pressure in LS, and causes the pure DPPC film remaining at the interface to reach the ultra-low surface pressures desirable for healthy breathing [31]. The black dash dot curve demonstrates the isotherm obtained for DPPC:POPC lipids mixed with 1 wt % (10 μg/ml) of ECNs. We found that the surface pressure vs. area isotherms obtained overlapped completely with the pure DPPC:POPC system.

2.5.1.5 Isotherms of DPPC:POPG: Addition of anionic POPG with mixed alkyl chain saturation to the DPPC film caused both an increase in the fluidity of the membrane, as well as a net negatively charged lipid

monolayer. Figure 2.1E (red dashed curve) demonstrates that the LE/LC coexistence was found to occur at a surface pressure of about ~15-17 mN/m. Surface pressure vs. mean molecular area isotherms obtained from samples containing 1 wt % (10 µg/ml) ECNs, overlapped completely with the characteristic curves of the ECN-free control systems (black dash dot lines).

2.5.2 Compressibility Modulus: Figure 2 shows the compressibility modulus as a function of mean molecular area for all the five samples described above. As seen in Figure 2.2A, at high mean molecular areas (> 75 $Å^2$/molecule), the DPPC film demonstrated a gradual increase in the compressibility modulus to about 25 mN/m followed by a sharp dip at a mean molecular area of about 70 $Å^2$/molecule. Beyond this dip, the compressibility modulus remained constant at a very small value until it shot up to 190 mN/m corresponding to monolayer collapse. ECN (black dashed curve) did not cause any significant alterations in the compressibility modulus, except at collapse where the maximum compressibility modulus was found to be higher (by 50 mN/m) in case of the lipid film containing ECN. Additionally, the position of the peak compressibility value also shifted to lower mean molecular areas. Figure 2.2B shows the compressibility modulus for DPPG films before and after adding ECNs. For the control system (red dashed curve), the lack of a significant discontinuity signifies absence of a first order phase transition in this system [25]. Addition of ECN showed almost overlapping curves with the control, except the absolute value of the maximum compressibility modulus, which was higher for the control. Figure 2.2C shows that for the DPPC:DPPG mixed lipid system, no change in the compressibility modulus was observed after adding ECN. Moreover, the position of the maximum shifted to lower mean molecular areas. Figure 2.2D shows that the compressibility modulus of a DPPC:POPC film (red dashed curve) did not alter due to ECNs. Figure 2.2E shows that no significant changes occur in the DPPC:POPG (red dashed curve) monolayer mechanical properties due to interactions with the ECNs (black dash-dot line).

2.5.3: Fluorescence Images:

2.5.3.1 Fluorescence Images of DPPC monolayers incubated with ECNs: Figure 2.3A represents a typical set of images showing the domain morphology of a pure DPPC monolayer at two different surface pressures: 4 mN/m, representative of the LE phase and 9 mN/m, representative of the LE/LC coexistence phase. In the LE phase, homogeneous mixing of the lipid dye caused the film to appear uniformly bright. However, this landscape quickly changed with the introduction of ECNs. Images obtained by spreading DPPC solutions mixed with ECN showed clusters of small circular dark domains. Contrast in these images is due to the selective segregation of bulky dye molecules in the more fluid regions, being excluded from the well-packed condensed domains that appear dark [34, 35]. In the LE-LC co-existence region, the pure DPPC film showed kidney bean shaped domains characteristic of DPPC. However, films formed after adding ECNs to the lipid solution started to cause alterations in the domain morphology. The kidney bean shaped domains started to aggregate to form multi-lobed structures while the net area of condensed LC domains increased, as shown in Figure 2.6A.

2.5.3.2 Fluorescence Images of DPPG monolayers incubated with ECNs: Figure 2.3B shows fluorescence microscopy images of DPPG films at two different surface pressures (20 mN/m and 30 mN/m) before and after addition of 10 μg/ml ECNs. The images for the pure DPPG appeared dark because the film exists in a LC state at both of the surface pressures reported [25]. Our images show that adding ECNs caused the DPPG domains to reduce in size, but they were still very well packed. Further analysis of the changes in the LC domains is shown in Figure 2.7B.

2.5.3.3 Fluorescence Images of DPPC: DPPG monolayers incubated with ECNs: Since the effect of ECN interactions on lipid domain formation were significantly different in DPPC lipids compared to anionic DPPG films, we wanted to study what would happen when ECNs were introduced to a system containing both these lipids. Figure 2.4 is a representative set of images of our observations. We found that DPPC:DPPG films formed well-packed circular domains. Domains formed by DPPC:DPPG molecules

incubated with ECNs showed alterations in the size of the domains and also the domain packing, with more fluid regions being visible. Analysis of the domain size distribution (Figure 2.5) showed a decrease in the width of the domain size distribution and also a decrease in the minimum energy radius R_0. Further, Figure 2.7 B shows that in this lipid environment, the ECNs induced significant decrease in the condensed area fraction.

2.5.3.4 Fluorescence Images of DPPC: POPC monolayers incubated with ECNs: To further explore if the alteration in domain packing induced by the ECNs may be modulated by the presence of unsaturated lipids, we also studied the domain formation in a DPPC: POPC film. As noted before, the introduction of phospholipids with mixed alkyl chains like POPC increased the fluidity of monolayer when compared with a pure DPPC system, without altering the overall headgroup charge. Figure 2.6A summarizes our results at two different representative surface pressures (20 mN/m and 30 mN/m). The control systems indicate that the kidney-bean shaped domains characteristic of DPPC monolayers were still present, with more bright regions compared to a pure DPPC monolayer. Figure 2.7 shows that adding ECNs to the lipid solution caused alterations in both the domain shape and domain size distribution. At 30 mN/m, ECNs had similar effect as the pure DPPC system, where the domains developed fractals or spikes arising from the domains. Further, as shown in Figure 2.7B, the addition of ECNs to this system caused a decrease in the condensed area fraction of the domains.

2.5.3.5 Fluorescence Images of DPPC: POPG monolayers incubated with ECNs: Finally, to test the effect of both lipid membrane saturation and electrostatic interactions between the anionic lipids and the anionic ECNs, we tested the formation of lipid domains in DPPC:POPG films containing ECNs. Introduction of POPG to DPPC films causes the appearance of circular domains which are not as well packed as films containing disaturated PG lipids, as shown in Figure 2.6B. It is well known that unlike the DPPC:DPPG system, the POPG molecules occupy the more fluid LE phase, while the DPPC domains make up the LC domains. While the addition of ECN did not show any visual change in the domain shape or the overall

fluidity, an analysis of the domain size distribution (Figure 2.5) showed that ECNs induced an increase in the minimum energy domain radius, and a decrease in the width of the domain size distribution.

To further analyze the domain morphology of the different lipid systems, due to the presence of the ECN, we plot the change in the condensed domain fraction, as shown in Figure 2.7. A negative change indicates increase in the total condensed domain fraction, while positive values indicate a decrease. Interestingly, we find that apart from DPPC lipids (Figure 2.7A), all other lipid mixtures showed a decrease in the net dark domains (Figure 2.7B), although this value was almost negligible (~ 5%) for the DPPC:POPG mixture. We also calculated changes in the line tension of the two anionic lipid mixtures, as shown in Figure 2.9. We find that the presence of saturated PG lipids causes the ECNs to cause an increase in the line tension, while in the presence of unsaturated PG lipids, the line tension was found to decrease.

2.5.4 AFM Images of DPPC: DPPG and DPPC: POPG monolayers incubated with ECNs: Finally, in order to correlate the calculated changes in the line tension of the two anionic lipid mixtures with the location of the ECNs in the monolayers, we imaged the DPPC:DPPG and DPPC:POPG films transferred onto a mica substrate at a surface pressure of 20 mN/m. Figure 8 shows higher resolution images of the lipid domains in the absence (Figure 2.9A and 2.9B) and presence (Figure 2.9C and 2.9D) of ECNs. The light brown regions correspond to LC domains, while the dark brown regions correspond to LE regions. The highly ordered lipid tails in LC domains causes LC domains to be slightly higher than the LE regions. Moreover, as noted earlier, the saturated DPPC and DPPG molecules form well packed LC domains, while the unsaturated POPG lipids occupy LE regions. As a result, Figure 2.8A shows more LC domains, while the DPPC:POPG film in Figure 2.9C shows circular, but less condensed regions. Further, Figures 2.9C and 2.9D show the appearance of raised features of height 30-50 nm and size 200 to 400 nm in lipid films containing ECNs. TEM images and DLS measurements described earlier suggest that even though the size of the ECNs in the dry powder state is 5-10 nm, thermodynamics causes these particles to exist as aggregates of size greater than 200 nm. Therefore, in the AFM images, the pink regions of height greater 20 nm and size

greater than 200 nm are attributed to ECNs. A height analysis of some of the raised features in Figures 2.9C and 2.9D (E, F) are also presented for further information of the dimensions of these raised features. In case of the DPPC:DPPG films, these large raised features of height greater than 30 nm are away from the domain boundaries, whereas, for the DPPC:POPG films, these features appear along the domain boundaries. Figure 2.9C also shows a few raised features within the LC domains. However, a detailed height and size analysis shows that these regions within the LC domains are less than a couple of nanometers high (Fig 2.15), suggesting that these cannot be ECN aggregates that compose of spherical or diamond shaped particles of size 5-10 nm.

2.6 Discussion:

This research is motivated by the need to understand how lipid headgroup charge and lipid membrane fluidity modulate lipid/nanoparticle interactions leading to alterations in mechanical and structural properties of lipid monolayers. The effect of both positively and negatively charged nanoparticles on the packing of zwitterionic lipids have been explored both experimentally and theoretically [35, 36]. However, to the best of our knowledge, how the lipid membrane packing is altered by charged nanoparticles in zwitterionic, anionic or mixed zwitterionic/anionic lipids with differences in membrane fluidity is currently not well understood. Our experiments were designed to study both the effect of lipid headgroup charge and lipid chain saturation on lipid nanoparticle interactions. DPPC is the major phospholipid component of LS, while PG lipids form the second most abundant component in native LS. Moreover, native and synthetic LS also contain unsaturated lipids, to allow efficient adsorption of LS. Therefore, the lipids used in this study were carefully selected to represent these combinations. While the studies described here followed changes in the lipid domain packing due to incubation of lipid molecules with one concentration of ECNs (Fig 2.10, 2.11, 2.12) also show the effect of an order of magnitude higher ECN concentration on these biophysical characteristics. Even though the thermodynamic properties of the lipids are not always

significantly affected by the ECNs, both the lipid headgroup charge and lipid alkyl chain saturation can dramatically influence the overall lipid domain shape and size in these systems. Our results conclusively establish that in addition to the surface properties of nanoparticles, the biophysical properties of the lipid compositions can also significantly influence the nanoparticles tendency to alter the phospholipid packing. Below we discuss our results in more detail.

2.6.1 Effect of lipid headgroup charge on lipid/ECN interactions in pure lipid systems: DPPC monolayers, with well characterized monolayer phases, were used as an example of a zwitterionic lipid with a net neutral charge, while DPPG was used as our model anionic lipid. The thermodynamic properties of both these systems are well characterized. The tail length of both these systems were chosen to be the same to ensure that the difference in lipid/nanoparticle interaction in these two pure systems is only as a result of differences in electrostatic interactions between the anionic ECNs and the net neutral or anionic phospholipid headgroups. While the isotherms for the DPPC films before and after adding ECNs did not show any significant alterations, the compressibility modulus slightly shifted to lower mean molecular areas and showed an increase in the maximum compressibility modulus. This increase implies that exposure with ECNs affected the overall mechanical properties of the DPPC films, and caused a possible condensation of the lipid domains. This possibility was explored further using fluorescence microscopy. Fluorescence microscopy is used to monitor molecular organization of lipid molecules in lipid monolayers [36], and the morphology of DPPC monolayers is now well established [28,37]. By comparing the domain morphologies of DPPC films before and after adding ECNs, we found that ECNs caused early nucleation of lipid domains. Further, an increase in the net condensed area was also measured, further confirming that the ECN caused a condensation of the lipid domains. Such an observation was also reported by Tatur and Badia, even though the physicochemistry of their gold nanoparticles is significantly different from our ECNs [31]. We also found that ECNs caused the characteristic bean-shaped domains of zwitterionic DPPC films to form more aggregated multilobed domains. Shape alteration in DPPC films from a kidney bean

structure to a more stretched out spiral structure indicates a lowering of the line tension between the LC domains and the surrounding LE regions [28, 38]. Such an alteration in domain shape has previously been reported when small amounts of cholesterol were added to a pure DPPC film [28,39]. Galla and co-workers found a similar effect with hydrophobic polymeric nanoparticles [9], while Tatur and Badia observed a similar effect when studying interactions between alkylated Au NPs and DPPC films, where AFM images showed the presence of aggregates of AuNPs around condensed DPPC domains [21]. The lowering of line tension indicates that like the hydrophobic polymeric and gold nanoparticles, ECNs act as line active species that prefer to associate with grain boundaries in saturated zwitterionic lipid films, thus altering the phospholipid packing in these systems.

Comparing the results for the effect induced by ECNs on a pure zwitterionic system compared to a pure anionic system like DPPG, we found that the isotherms and compressibility moduli overlapped completely for the systems with and without ECN, except that a decrease in the maximum compressibility modulus was noted. These observations suggest that the thermodynamic properties of the DPPG films were not affected by exposure to ECN, but the compressibility modulus was decreased, suggesting a slight increase in the membrane fluidity. Similarly, no significant changes were observed in the shape of well-packed large lipid domains of DPPG, after exposure to the ECNs. However, careful analysis of the condensed area fraction did show that ECN induced a decrease (~20%) in the total fraction of dark domains, indicating an increase in the membrane fluidity. McConell and co-workers have previously shown that domain morphologies are determined by a balance between the line tension between domains and electrostatic energies resulting from dipole interactions between domains [38]. The tendency to minimize line tension causes long stretched out domains, while minimizing dipole interactions causes break-up of larger domains into smaller sizes. Even though the domains were still well packed for the DPPG films, the decrease in the overall dark condensed domains, as well as the lack of spiral or multilobed domains in case of pure DPPG suggest that for the pure anionic saturated phospholipid systems these ECNs are no

longer line active species, but rather increase the overall fluidity of the monolayers. However, this change was subtle enough that it could not be detected in the compressibility isotherm.

2.6.2 Effect of lipid headgroup charge and membrane packing on lipid/ECN interactions in mixed lipid systems: To further prove that the differences in the changes in lipid domain shape and size distribution induced by ECN was due to differences in the interactions with the different lipid headgroups, DPPC: DPPG (7:3) was used as a mixed saturated lipid system. In this system, the LC domains are net negatively charged, because of the tendency of DPPG to form LC phases even at very low surface pressure. If our hypothesis, stated above, is correct, we would expect that the anionic ECNs would be repelled by the anionic LC domains, causing an increase in the membrane fluidity. Further, repulsion from the domain boundaries would cause ECN to increase the line tension, due to repulsion from the lipid domain boundary [31]. Indeed, we experimentally measured that the ECNs induced a decrease in the condensed area fraction of domains. We also measured an increase in the line tension between domains for the DPPC:DPPG system, suggesting that the ECNs avoid the line boundaries. To further confirm this, we replaced DPPG with POPG molecules. Since POPG is unsaturated, unlike the DPPG molecules, it is expected to occupy the LE phases in the monolayer [31]. According to our explanation, this would suggest that in the presence of POPG, the ECNs would avoid the fluid LE phases and continue to prefer the condensed DPPC domains, which in turn would cause a lowering of the line tension. Indeed, we do measure a decrease in the line tension between domains for the DPPC:POPG films. This observation is also expected based on our previous observations of lipid-protein interactions [31]. We have previously reported that positively charged proteins caused an increase in line tension between domains in a clinical lung surfactant mixture, where the POPG molecules occupy the fluid LE regions. Finally, our AFM images provide concrete evidence of this hypothesis. Careful analysis of the location of raised features of height 20 nm or greater and sizes greater than 200 nm conclusively established that indeed the sub-micron sized ECN aggregates prefer the fluid LE phase in case of the DPPC:DPPG films, while they avoid the anionic LE phase and prefer

the LC domain boundaries in case of the DPPC:POPG films. Further, our data (Fig 2.12) shows that at higher ECN concentrations, the nanoparticles do cause a visible breaking of the circular domains into spirals, suggesting a further lowering of line tension. Similarly, changing the sub-phase from water to buffer accentuates the lowering of the line tension in DPPC:POPG films, as shownFig 2.14. Finally, we expect that if the LC domains retain their zwitterionic charge, the ECNs will continue to demonstrate their line active behavior. Again, this is what was experimentally observed for the DPPC:POPC monolayers. We observed that ECNs caused a decrease in the total condensed area as well, indicating that in the presence of unsaturated lipids, the ECNs lose their ability to nucleate and condense the DPPC domains. The reason for this is currently unclear, although one possibility is that at lower surface pressures the ECNs coexist with the unsaturated lipids, and are hence unable to serve as nucleation sites for domain condensation. Since the lipid morphology and line tension between domains have been shown to be related to the ability of lung surfactant films to resist collapse at ultra-low surface tensions, potential for re-adsorption and respreading of lipid material after monolayer collapse, as well as membrane curvature in lipid bilayers (which in turn can be related to the stability of membranes) [31], we hypothesize that the same nanoparticles can demonstrate significantly different effects on the biophysical performance of different model lipid mixtures. Therefore, our results suggest that when reporting the potential adverse effects of nanoparticles, one should also consider the lipid headgroup charges, alkyl chain saturation and their effect on lipid/nanoparticle interactions.

2.7 Conclusion:

In conclusion, we report that phospholipid headgroup charge, lipid composition and lipid alkyl chain saturation modulate nanoparticle induced changes in lipid systems. We found that anionic ECNs were line active and interacted with lipid domain boundaries resulting in a lowering of line tension, when present in a zwitterionic environment. This observation is in line with prior results with hydrophobic metallic and polymeric particles. In addition, we found that in the presence of anionic phospholipids, electrostatic

repulsion between the domains dominated, and controlled the alterations in lipid domain packing induced by the ECNs, even in a mixed system with an excess composition of the zwitterionic lipid. While the effect of nanoparticles of different surface charge, surface modification and size on the packing of phospholipids have been described before, we present, for the first time, a controlled study to understand how physicochemical properties of lipids modulate lipid nanoparticle interactions.

2.8 FIGURES:

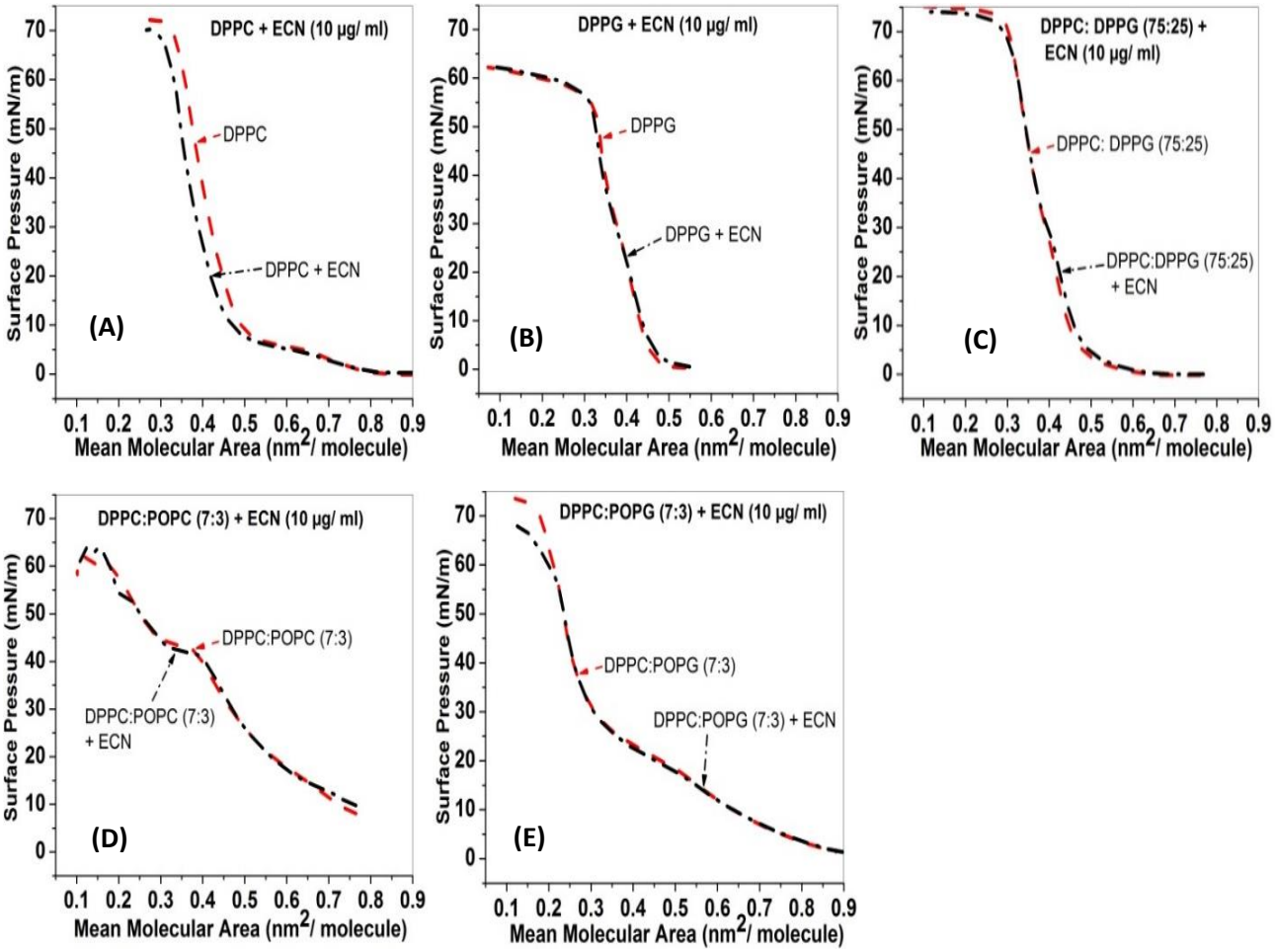

Figure 2.1: Surface Pressure vs. mean molecular area isotherms for (A) a DPPC (B) DPPG (C) DPPC:DPPG (75:25) (D) DPPC:POPC (7:3) (E) DPPC:POPG (7:3) monolayers containing 1 wt % (10 µg/ml) ECN.

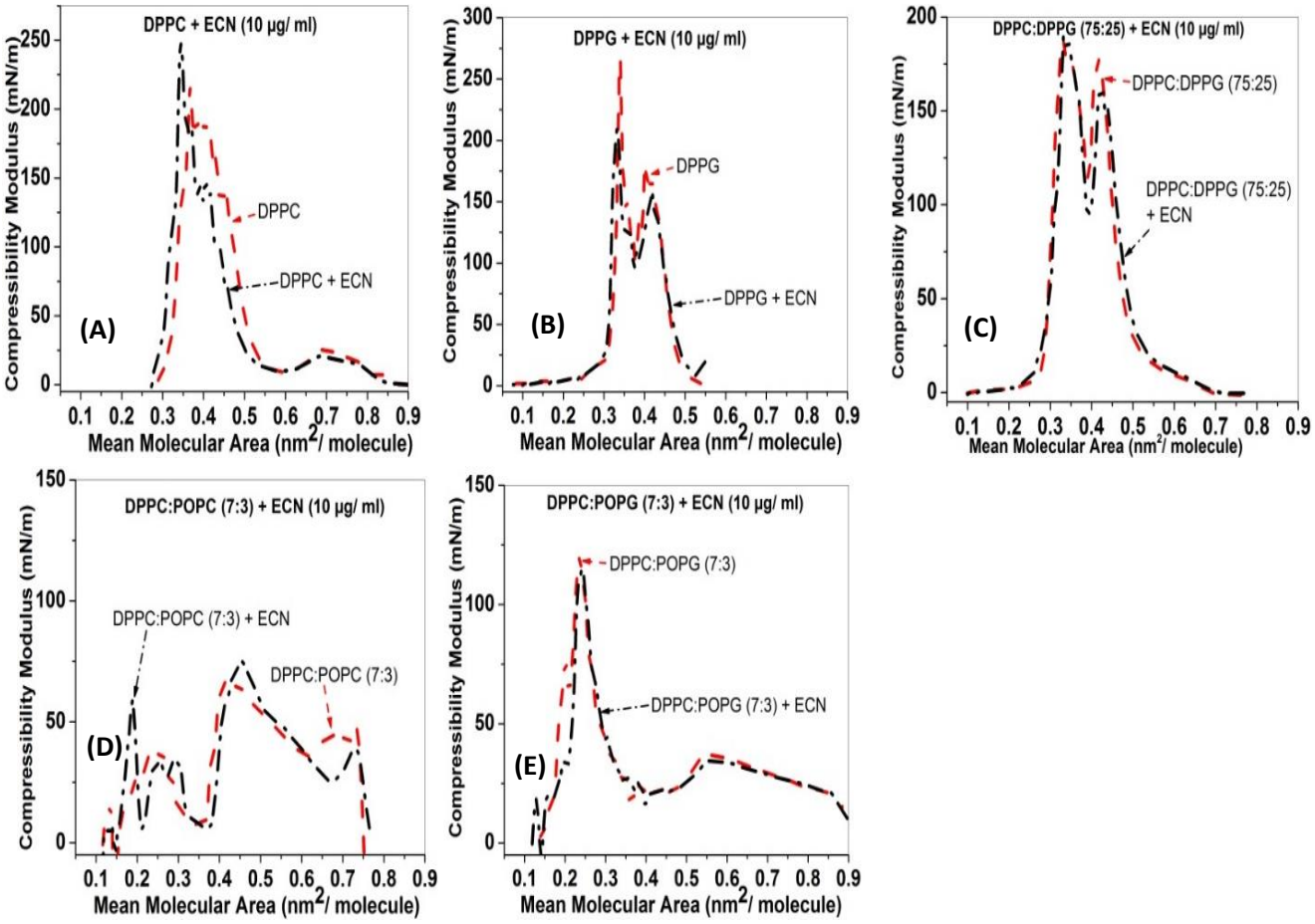

Figure 2.2: Compressibility Modulus vs. mean molecular area isotherms for (A) a DPPC (B) DPPG (C) DPPC:DPPG (75:25) (D) DPPC:POPC (7:3) (E) DPPC:POPG (7:3) monolayers containing 1 wt % (10 µg/ml) ECN.

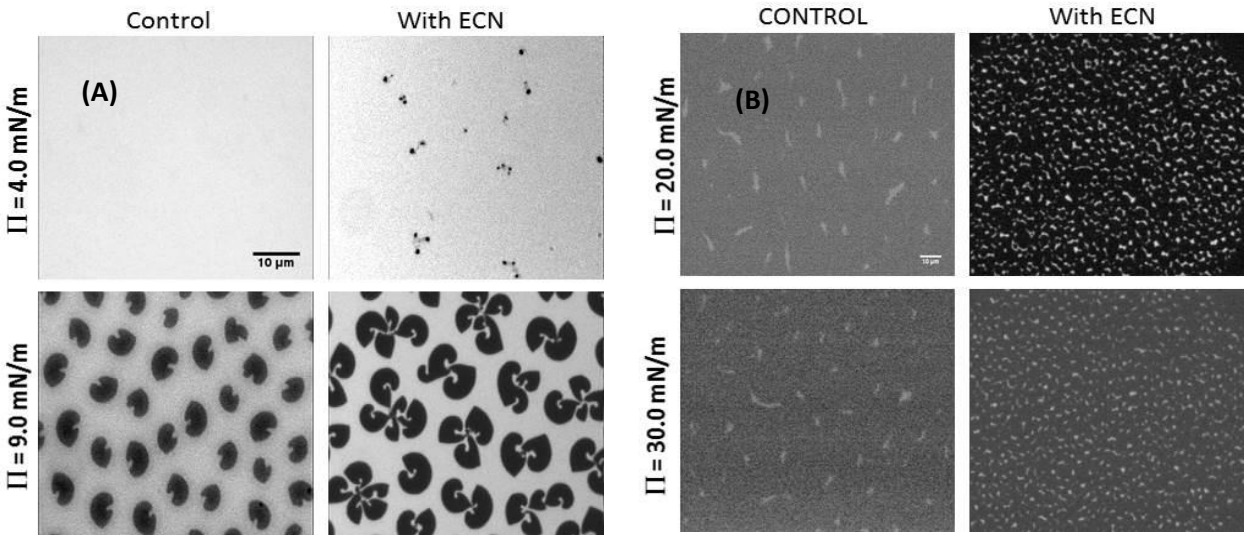

Figure 2.3: Fluorescence Microscopy images of pure (A) DPPC and (B) DPPG monolayers before (Control) and after adding 1 wt % (10 µg/ml) ECN, at two representative surface pressures. Contrast in these images is due to the selective segregation of bulky phospholipid modified dye molecules into the more fluid regions. The kidney bean structures, characteristic of a pure DPPC system, underwent drastic transitions to more spiral shape due to interactions with the ECNs. The scale bar is 10µm.

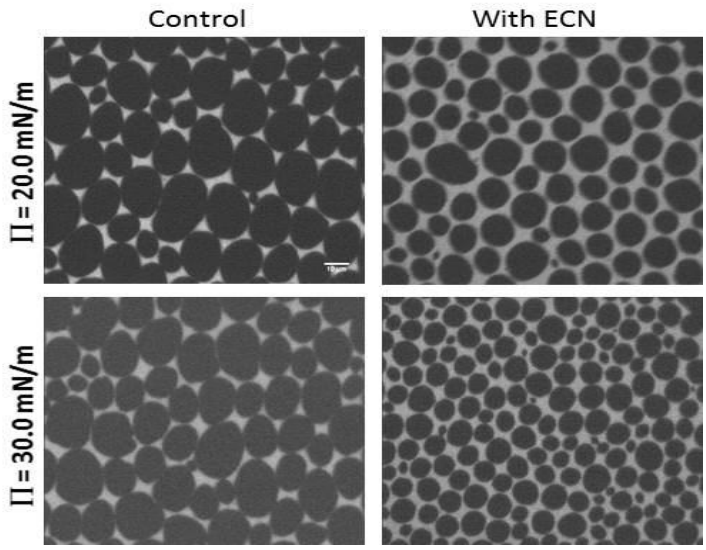

Figure 2.4: Fluorescence Microscopy images of a mixed DPPC:DPPG (75:25) monolayer with a net anionic charge before (Control) and after adding 1 wt % (10 μg/ml) of anionic ECNs. A decrease in the domain size, and increase in number density was noted (Fig 2.13), but unlike a pure DPPC film, no change in the shape of the domains was observed. The scale bar is 10 μm.

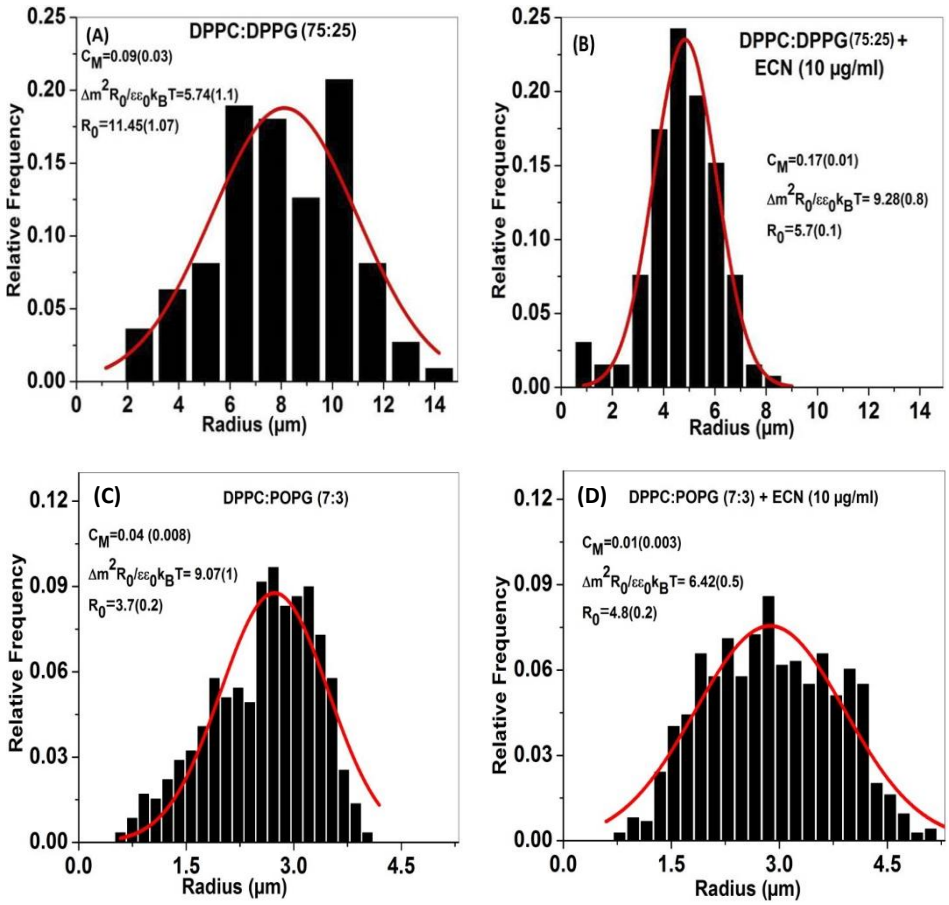

Figure 2.5: Analysis of domain size distribution of DPPC:DPPG and DPPC:POPG monolayers in the absence (A,C) and presence (B,D) of ECNs. The red curve shows the fit to Equation 4 in the main text. The curve fitting yielded an average adjusted R-Squared value of 0.87, indicating the good quality of the fit. The fitting parameters are also shown.

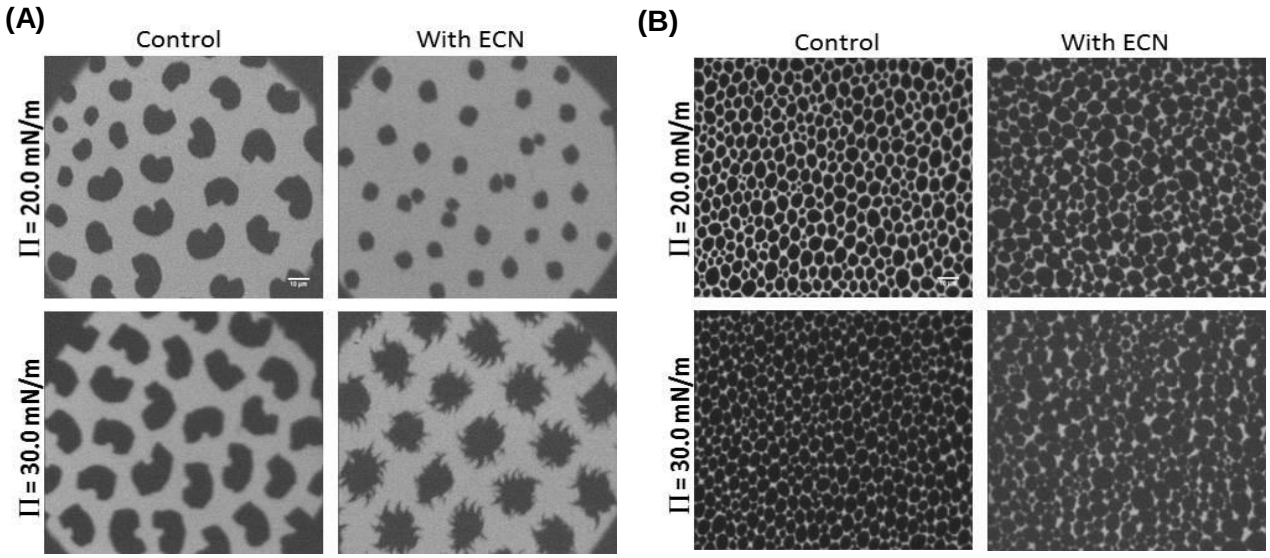

Figure 2.6: Fluorescence Microscopy images of a mixed (A) DPPC:POPC (7:3) monolayer with a net neutral charge and (B) DPPC:POPG (7:3) monolayer with a net anionic charge and unsaturated lipids before (Control) and after adding 1 wt % (10 μg/ml) of anionic ECNs. The scale bar is 10 μm.

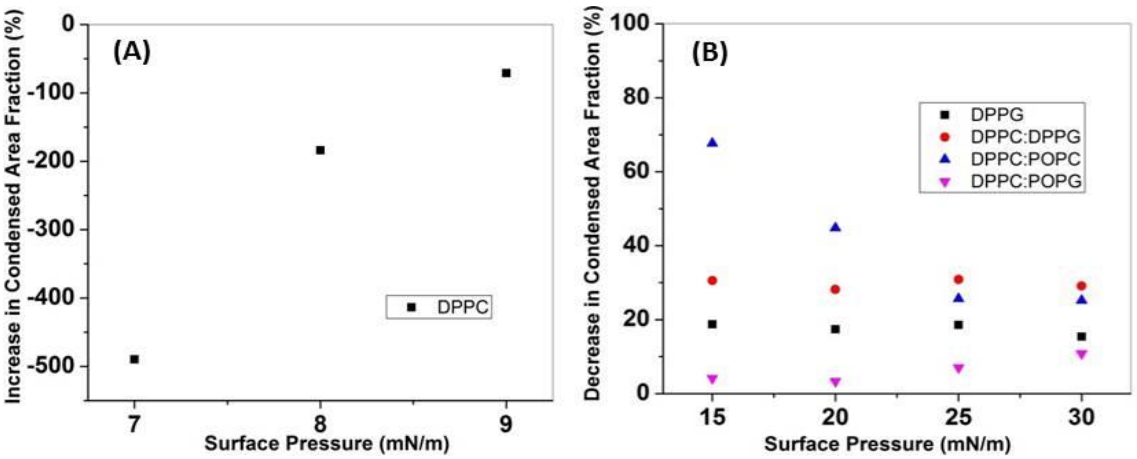

Figure 2.7: Change in the condensed area fraction with the addition of ECN as a function of surface pressure. Positive values indicate a lowering in the area of the condensed region whereas a negative value refers to an increase in the area. (A) For DPPC, there was an increase in the domain area with the introduction of ECN and the change decreased sharply with the increase in surface pressure. (B) In case of DPPG, the condensed area fraction reduced as the negatively charged domains repelled the nanoparticles. A similar trend was observed for DPPC:DPPG. For DPPC:POPC, we recorded the highest reduction in area, but the change decreased with an increase in the surface pressure. Finally, we found very little change in the area for DPPC:POPG.

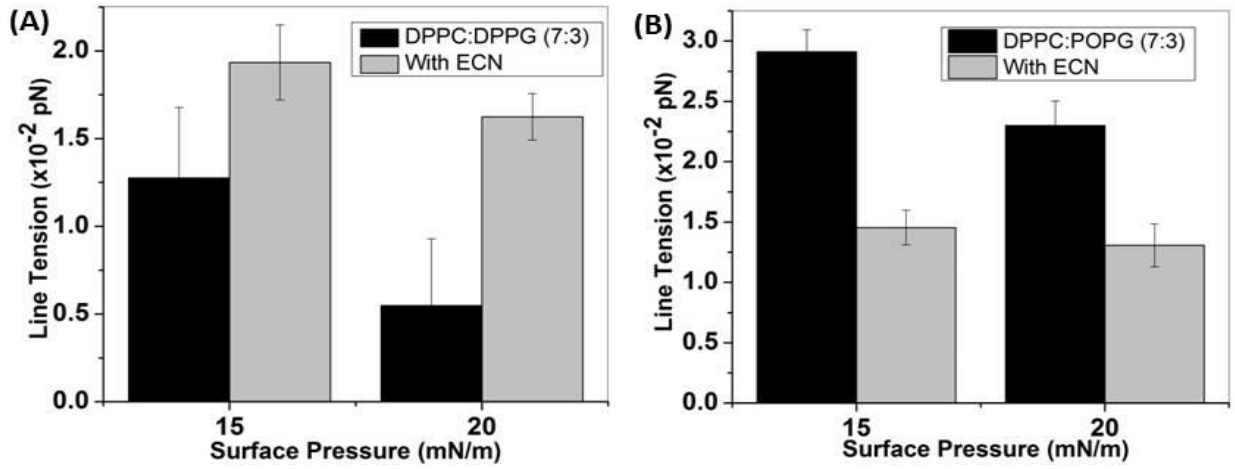

Figure 2.8: Changes in the line tension of (A) DPPC:DPPG and (B) DPPC:POPG at two different surface pressures in the absence and presence of 1 wt % (10 µg/ml) of ECN.

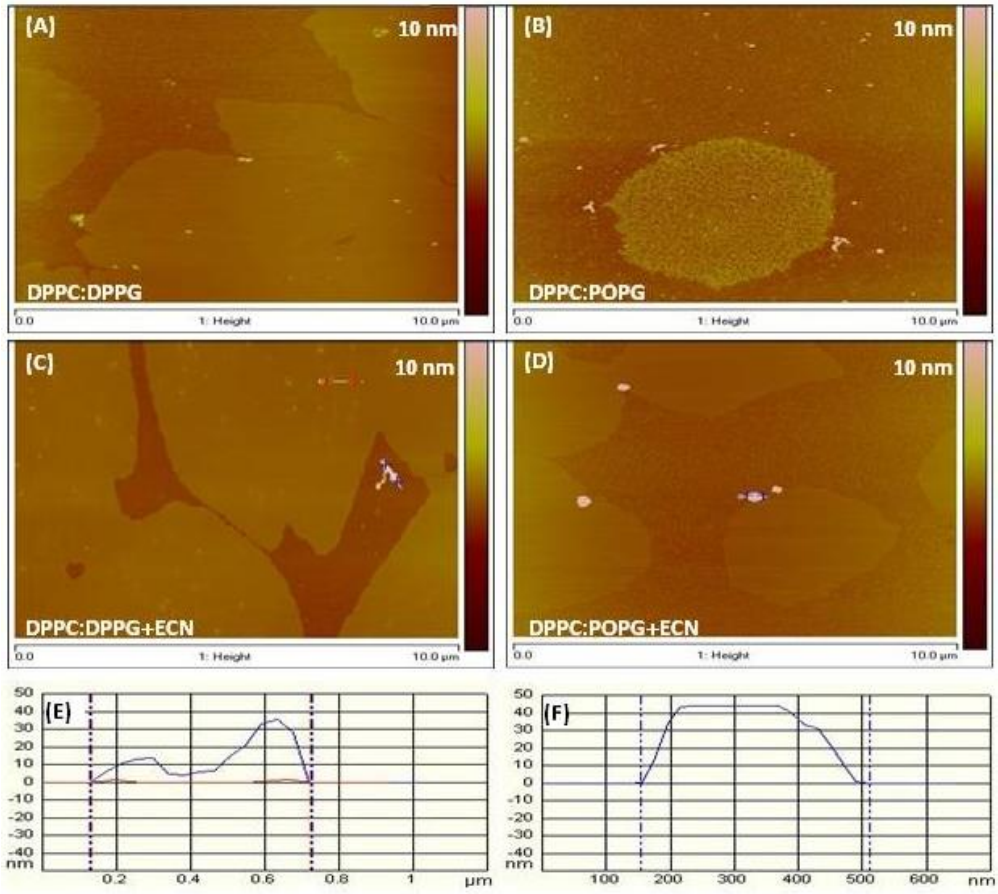

Figure 2.9: AFM images of the net anionic binary mixtures of phospholipid films transferred onto a solid mica substrate. (A, B): DPPC:DPPG films in the absence and presence of ECN respectively (C,D): DPPC:POPG films in the absence and presence of ECN respectively. (E,F) Show the height analysis of the raised features indicated by white lines in B and D.

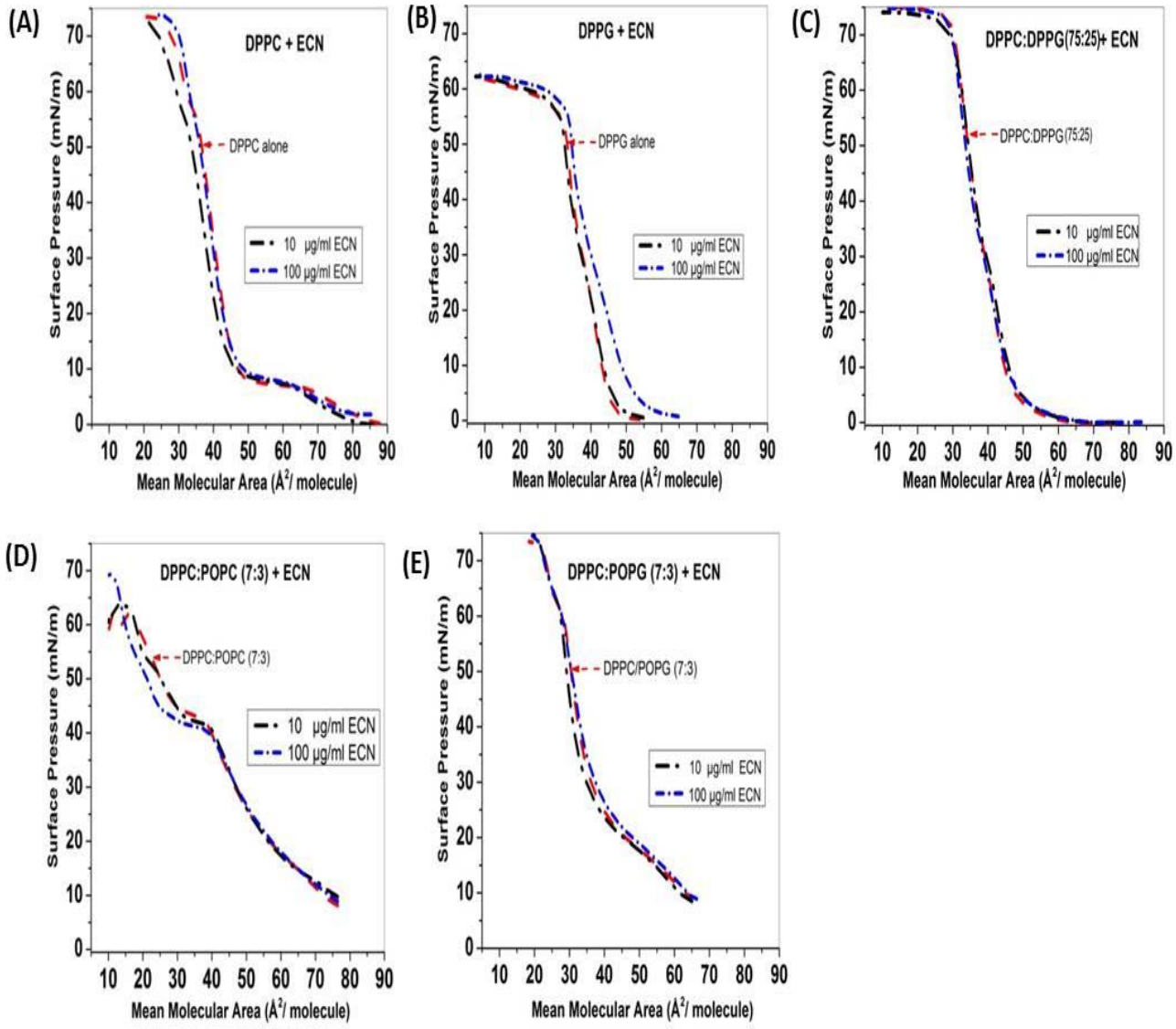

Figure 2.10: Surface Pressure vs. area per molecule isotherms of (A) DPPC (B) DPPG (C) DPPC: DPPG (75:25) (D) DPPC:POPC (7:3) (E) DPPC:POPG (7:3) monolayers obtained after one hour of incubation with 1 wt % (10 µg/ml) and 10 wt% (100 µg/ml) ECN.

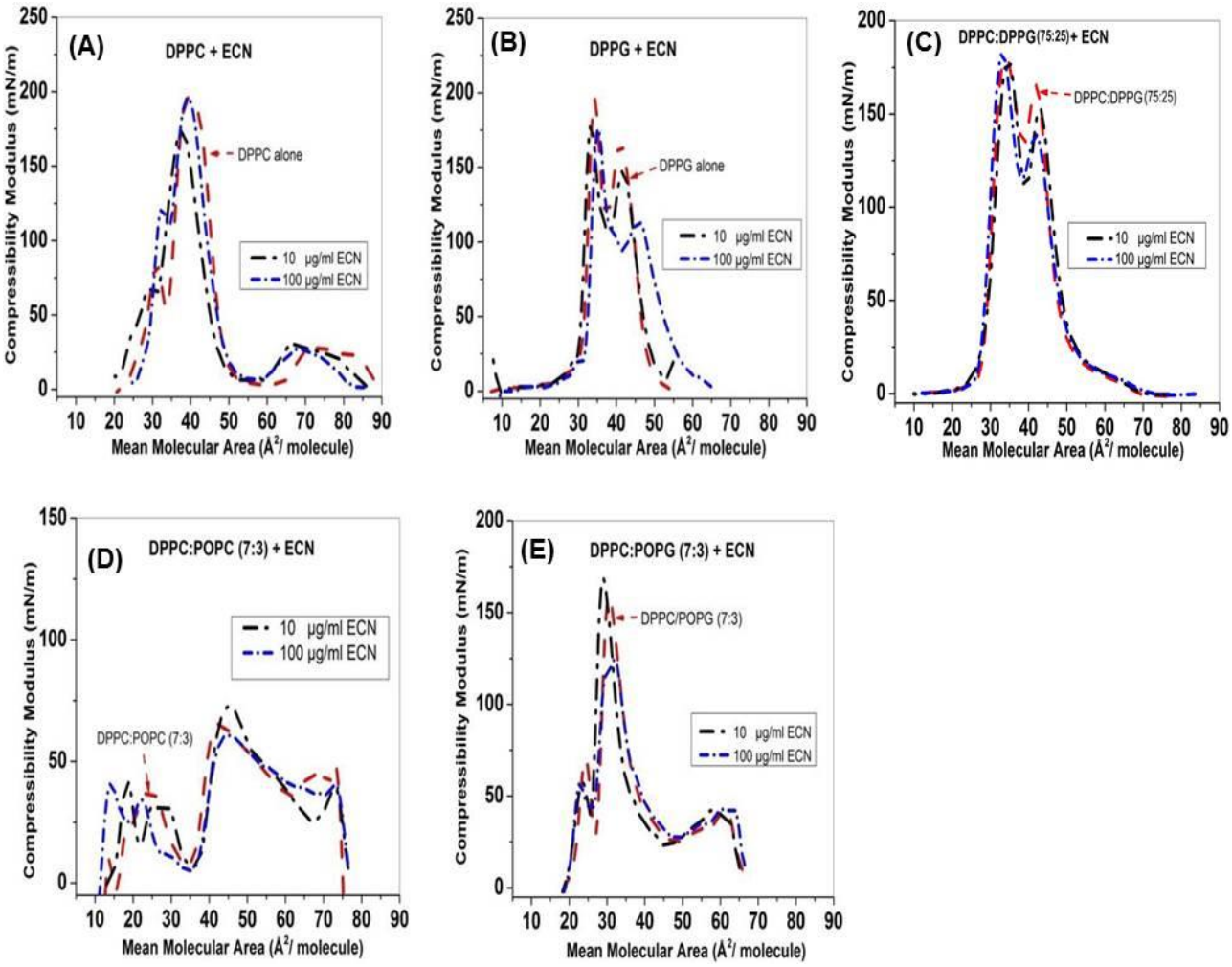

Figure 2.11: Compressibility Modulus vs. area per molecule isotherms for (A) DPPC (B) DPPG (C) DPPC: DPPG (75:25) (D) DPPC:POPC (7:3) (E) DPPC:POPG (7:3) monolayers obtained after one hour of incubation with 1 wt % (10 mg/ml) and 10 wt% (100µg/ml) ECN.

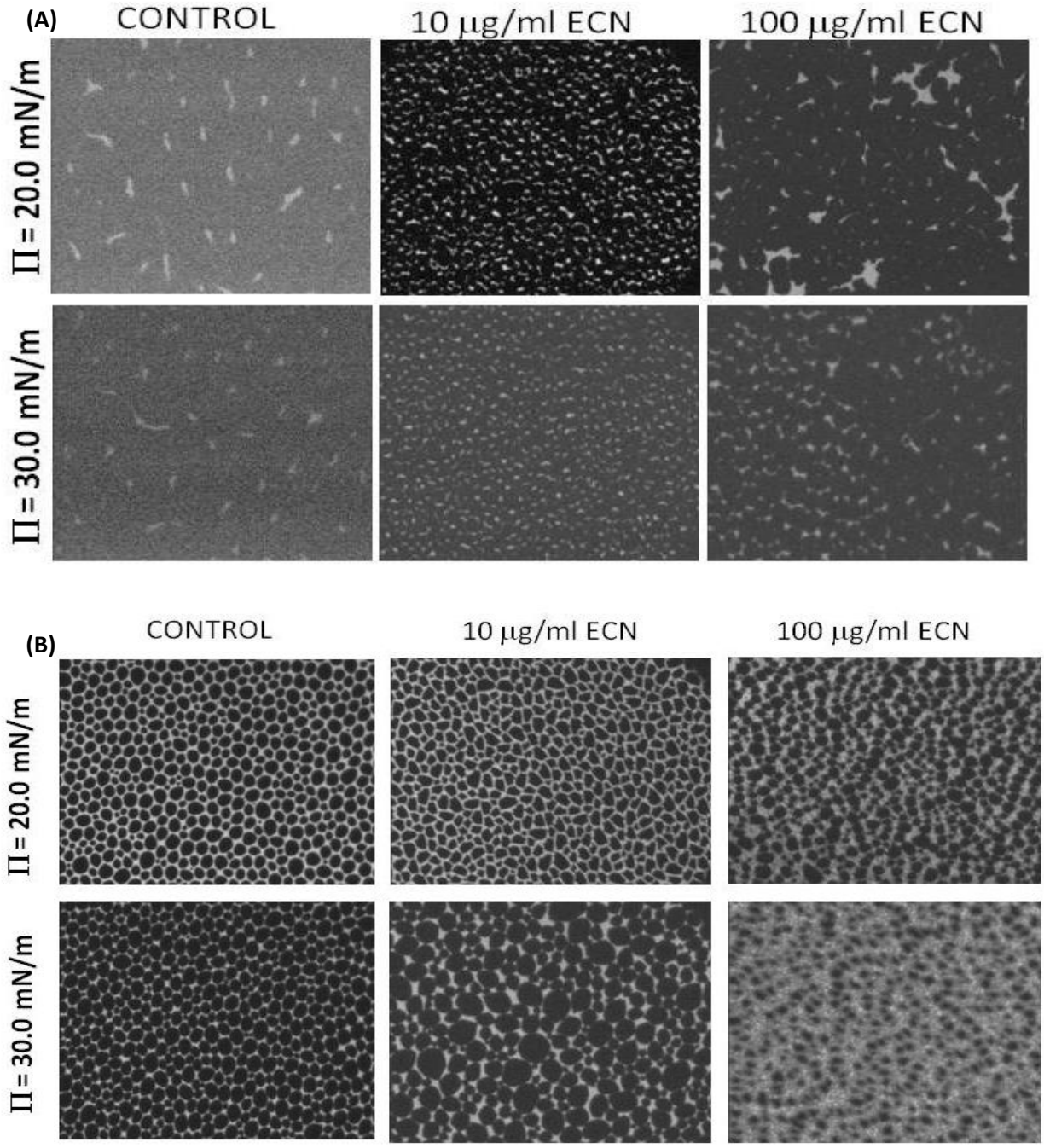

Figure 2.12: Comparison of ECN induced alterations in lipid domains as a result of exposure to different concentrations of ECN (A) DPPG (B) DPPC:POPG mixture.

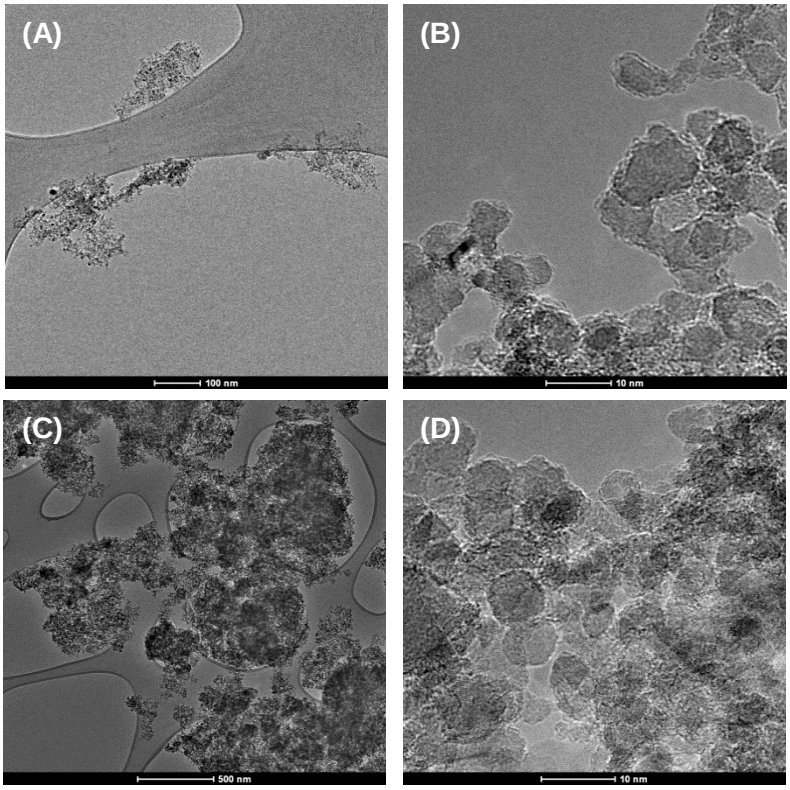

Figure 2.13: TEM images of the ECNs originally suspended in water (A and B) and organic solvent (C and D) show that the ECNs have a tendency to aggregate into sub micron particle size in media, even though they are about 5-10 nm in the dry powder state. The aggregates show these individual particles in higher resolution images (B and D). Scale: A: 100 nm, B, D: 10 nm, C: 500 nm.

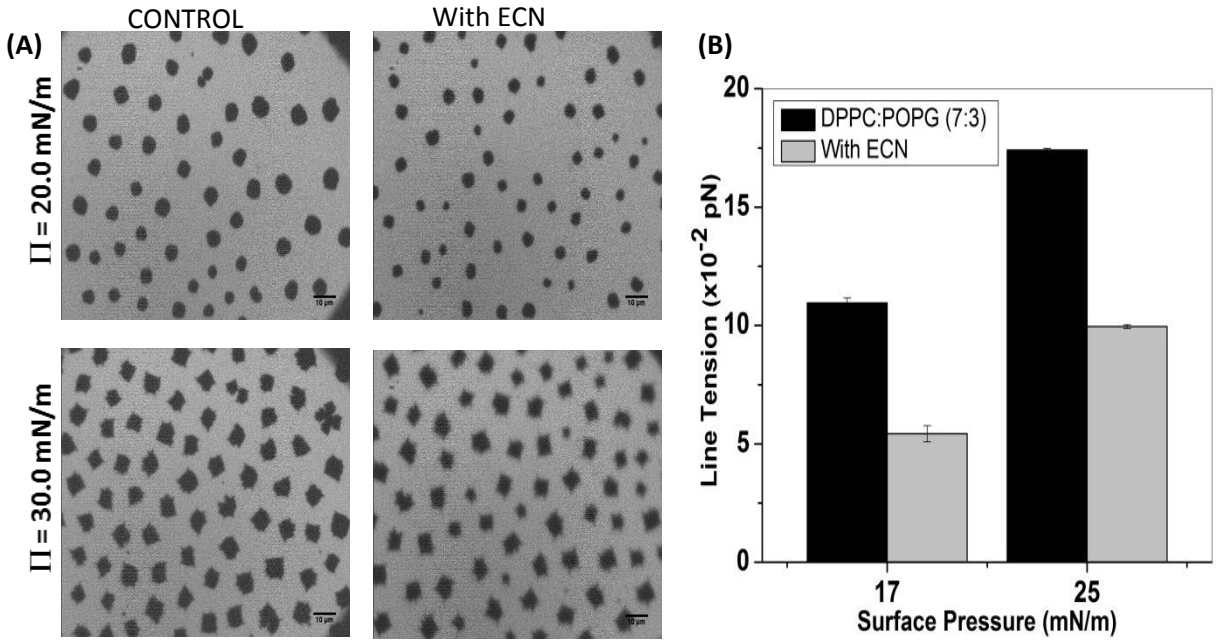

Figure 2.14: (A) Fluorescence images of DPPC:POPG films without and with ECN spread on a PBS buffer sub-phase at two representative surface pressures. (B) Line tension analysis from the domain size distributions in (A) show a significant decrease in the line tension in the presence of ECNs.

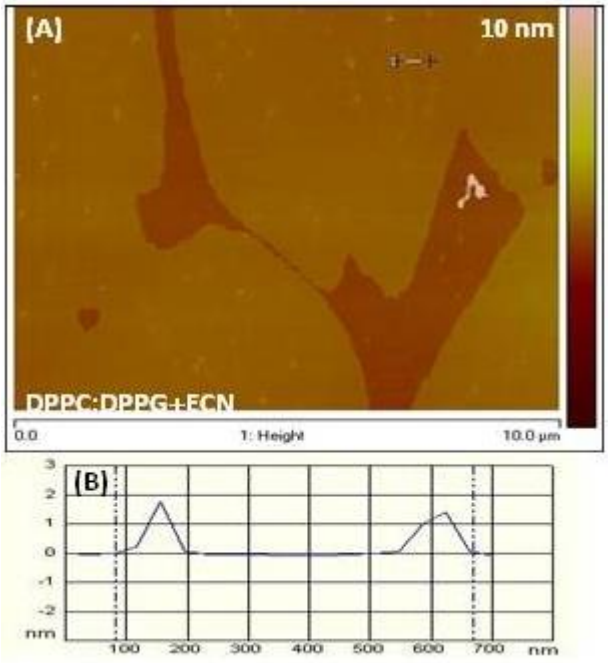

Fig 2.15: Detailed height analysis within a condensed domain shows that unlike the significant height change in the LE phase, the raised features within the LC domain do not correspond to ECN aggregates of size ~ 250 nm, since the height of these features is significantly lower than that expected for ECN aggregates that contain carbon nanodiamonds of diameter 5-10 nm.

2.9 References:

1. Sharifi, S., et al., *Toxicity of nanomaterials.* Chemical Society Reviews, 2012. **41**(6): p. 2323-2343.
2. Dawson, K.A., et al., *Nanotoxicology: nanoparticles reconstruct lipids.* Nat Nanotechnol, 2009. **4**(2): p. 84-5.
3. Love, S.A., et al., *Assessing nanoparticle toxicity.* Annu Rev Anal Chem (Palo Alto Calif), 2012. **5**: p. 181-205.
4. Kapralov, A.A., et al., *Adsorption of Surfactant Lipids by Single-Walled Carbon Nanotubes in Mouse Lung upon Pharyngeal Aspiration.* ACS Nano, 2012. **6**(5): p. 4147-4156.
5. Kendall, M. and S. Holgate, *Health impact and toxicological effects of nanomaterials in the lung.* Respirology, 2012. **17**(5): p. 743-758.
6. Schleh, C., et al., *Pulmonary surfactant is indispensable in order to simulate the in vivo situation.* Particle and Fibre Toxicology, 2013. **10**.
7. Warheit, D.B., *How meaningful are the results of nanotoxicity studies in the absence of adequate material characterization?* Toxicological Sciences, 2008. **101**(2): p. 183-185.
8. Heyder, J., *Deposition of inhaled particles in the human respiratory tract and consequences for regional targeting in respiratory drug delivery.* Proc Am Thorac Soc, 2004. **1**(4): p. 315-20.
9. Harishchandra, R.K., et al., *Nanoparticle interaction with model lung surfactant monolayers.* J R Soc Interface, 2010. **7 Suppl 1**: p. S15-26.
10. Sachan, A.K., et al., *High-resolution investigation of nanoparticle interaction with a model pulmonary surfactant monolayer.* ACS Nano, 2012. **6**(2): p. 1677-87.
11. Sachan, A.K., et al., *Understanding the mutual impact of interaction between hydrophobic nanoparticles and pulmonary surfactant monolayer.* Small, 2014. **10**(6): p. 1069-75.
12. Dwivedi, M.V., et al., *Size influences the effect of hydrophobic nanoparticles on lung surfactant model systems.* Biophys J, 2014. **106**(1): p. 289-98.
13. Fan, Q., et al., *Adverse biophysical effects of hydroxyapatite nanoparticles on natural pulmonary surfactant.* ACS Nano, 2011. **5**(8): p. 6410-6.
14. Hu, G., et al., *Physicochemical Properties of Nanoparticles Regulate Translocation across Pulmonary Surfactant Monolayer and Formation of Lipoprotein Corona.* ACS Nano, 2013. **7**(12): p. 10525-33.
15. Beck-Broichsitter, M., et al., *Biophysical investigation of pulmonary surfactant surface properties upon contact with polymeric nanoparticles in vitro.* Nanomedicine, 2011. **7**(3): p. 341-50.
16. Farnoud, A.M., et al., *Surfactant Interactions with Sub-Micron Particles: The Importance of Route of Exposure.* Journal of Aerosol Medicine and Pulmonary Drug Delivery, 2013. **26**(2): p. A60-A61.
17. Schleh, C., et al., *The effect of titanium dioxide nanoparticles on pulmonary surfactant function and ultrastructure.* Respiratory Research, 2009. **10**.
18. Schleh, C., et al., *Titanium Dioxide Nanoparticles Alter Pulmonary Surfactant Ultrastructure and Biophysical Function.* American Journal of Respiratory and Critical Care Medicine, 2009. **179**.
19. Kodama, A.T., et al., *Investigating the effect of particle size on pulmonary surfactant phase behavior.* Biophys J, 2014. **107**(7): p. 1573-81.
20. Bakshi, M.S., et al., *Metal nanoparticle pollutants interfere with pulmonary surfactant function in vitro.* Biophysical Journal, 2008. **94**(3): p. 855-868.
21. Tatur, S., et al., *Influence of Hydrophobic Alkylated Gold Nanoparticles on the Phase Behavior of Monolayers of DPPC and Clinical Lung Surfactant.* Langmuir, 2012. **28**(1): p. 628-639.
22. Mochalin, V.N., et al., *The properties and applications of nanodiamonds.* Nat Nanotechnol, 2012. **7**(1): p. 11-23.

23. Zhang, T., et al., *Photoacoustic imaging of biological tissues with radiation damaged nanodiamonds as a near infrared optical contrast agent.* Journal of Biomedical Optics, 2013. **18**(2): p. 26018
24. Zhang, T., et al., *Targeted nanodiamons as phenotype specific photoacoustic contrast agents for breast cancer.* Nanomedicine, Accepted, 2014.
25. Vollhardt, D., et al., *Thermodynamic and textural characterization of DPPG phospholipid monolayers.* Journal of Physical Chemistry B, 2000. **104**(17): p. 4115-4121.
26. Farnoud, A.M., et al., *Interaction of dipalmitoyl phosphatidylcholine monolayers with a particle-laden subphase.* Journal of Physical Chemistry B, 2013. **117**(40): p. 12124-34.
27. Knobler, C.M., *SEEING PHENOMENA IN FLATLAND - STUDIES OF MONOLAYERS BY FLUORESCENCE MICROSCOPY.* Science, 1990. **249**(4971): p. 870-874.
28. Mcconnell, H.M., *Structures and Transitions in Lipid Monolayers at the Air-Water-Interface.* Annual Review of Physical Chemistry, 1991. **42**: p. 171-195.
29. Benvegnu, D.J., et al.,*LINE TENSION BETWEEN LIQUID DOMAINS IN LIPID MONOLAYERS.* Journal of Physical Chemistry, 1992. **96**(16): p. 6820-6824.
30. Benvegnu, D.J., et al., *SURFACE DIPOLE DENSITIES IN LIPID MONOLAYERS.* Journal of Physical Chemistry, 1993. **97**(25): p. 6686-6691.
31. Dhar, P., et al., *Lipid-protein interactions alter line tensions and domain size distributions in lung surfactant monolayers.* Biophys J, 2012. **102**(1): p. 56-65.
32. Lee, D.W., et al., *Relating domain size distribution to line tension and molecular dipole density in model cytoplasmic myelin lipid monolayers.* Proc Natl Acad Sci U S A, 2011. **108**(23): p. 9425-30.
33. Lee, K.Y.C., et al., *Apparatus for the continuous monitoring of surface morphology via fluorescence microscopy during monolayer transfer to substrates.* Langmuir, 1998. **14**(9): p. 2567-2572.
34. Mohwald, H., *Phospholipid and phospholipid-protein monolayers at the air/water interface.* Annu Rev Phys Chem, 1990. **41**: p. 441-76.
35. Velikonja, A., et al., *Interaction between Dipolar Lipid Headgroups and Charged Nanoparticles Mediated by Water Dipoles and Ions.* International Journal of Molecular Sciences, 2013. **14**(8): p. 15312-15329.
36. Wang, B., et al., *Nanoparticle-induced surface reconstruction of phospholipid membranes.* Proceedings of the National Academy of Sciences of the United States of America, 2008. **105**(47): p. 18171-18175.
37. McConlogue, C.W., et al., *A close look at domain formation in DPPC monolayers.* Langmuir, 1997. **13**(26): p. 7158-7164.
38. Keller, S.L., et al.,*Stripe phases in lipid monolayers near a miscibility critical point.* Physical Review Letters, 1999. **82**(7): p. 1602-1605.
39. Kim, K., et al., *Effect of cholesterol nanodomains on monolayer morphology and dynamics.* Proc Natl Acad Sci U S A, 2013. **110**(33): p. E3054-60.

Chapter 3

Synthetic Protein, MiniB, Counters the Effect of Cholesterol in a Simple Binary Mixture of Lung Surfactant Phospholipids at the Air-Water Interface

3.1 Abstract:

Lung surfactants [LS], a complex mixture of lipids and proteins, play a crucial role in lowering the line tension at the air-water interface in the alveoli of the lungs, reducing the work needed for breathing and also improving lung compliance. A deficiency/ impairment of the lung surfactants may prove to be fatal making medical intervention with Surfactant Replacement Therapy [SRT] absolutely vital in such cases. However, there is yet to be a consensus on the composition of LS used in SRT, especially the interaction between the various components of the mixture. We aimed at understanding how Mini B, a synthetic analog of SPB, a hydrophobic surfactant protein, interacts with cholesterol, which is a highly debated component, in the presence of a simple binary mixture of LS phospholipids, namely, 1,2-dipalmitoyl-*sn*-glycero-3-phosphocholine (DPPC) and 1-palmitoyl-2-oleoyl-*sn*-glycero-3-phospho-(1'-*rac*-glycerol) (POPG) in the weight ratio 7:3. Based on surface pressure versus mean molecular area isotherms and fluorescence imaging under constant compression, we conclude that a low concentration of Mini B along with an equal concentration of cholesterol aids in the proper functioning of synthetic LS. Cholesterol prefers to stretch out the phospholipid domains by lowering line tension and also makes LS collapse irreversibly. On the contrary, a domain size distribution analysis reveals that Mini B increases line tension between the domains. Mini B also helps LS to collapse reversibly forming giant folds, therefore, preventing material loss from the interface. A tug of war ensues as the two are put together and Mini B dominates at lower concentrations of the two. However, at higher concentration, cholesterol tends to dominate.

3.2 Introduction:

Lung surfactants [LS] are a complex mixture of lipids and proteins present primarily in the alveolar lining of the lungs, produced by Type II epithelial cells [1]. LS help in lowering surface tension at the air-water interface with expiration, thereby reducing the energy needed for breathing and improving lung compliance [2, 3]. They also form a line of defense against any foreign particle that is small enough to

make its way through the air canal.[4] It has been firmly established that there is a lack of LS in cases of Neonatal Respiratory Distress Syndrome [NRDS] occurring in infants.[5] On the other hand, a dysfunction/ impairment of the surfactant may lead to Acute Respiratory Distress Syndrome (ARDS)/ Acute Lung Injury (ALI) and each year, a staggering 50,000- 190,000 cases of ALI/ARDS are reported in USA itself.[6] Thus, the contribution of LS towards a healthy living is vital and the need to understand its composition is pivotal.

The bulk constituent of LS are the phospholipids which amount to around 80% whereas 5-10% are the neutral lipids and the rest are the surfactant proteins [7]. The Phospholipids mainly consists of the zwitterionic PhosphatidylCholine (PC), which is about 60-70%, whereas, the anionic PhosphatidylGlycerol (PG) and PhosphatidylInositol (PI) make up to 8-15%. [8] The saturated DPPC is efficient in lowering the values of surface tension to near zero as it forms well packed gel phase [9]. However, the unsaturated lipids are needed for adsorption[10] and respreading[11] as they render fluidity to the system. The neutral lipids primarily consist of cholesterol[12]. Although less in quantity, the surfactant proteins play a crucial part. The hydrophobic SPB and SPC are involved in enhancing adsorption of LS to the air-water interface, whereas, the hydrophilic SPA and SPD mainly play a part in immune response [13]. The knowledge of each component is essential for Surfactant Replacement Therapy (SRT).

Till date there is no consensus on the composition of the lung surfactant mixtures available for SRT [14]. Two major classes of LS, commercially available for SRT, are: a. animal derived (natural) surfactant and b. synthetic surfactant. The natural surfactants are primarily bovine or porcine. So far it has been shown that the natural surfactants are better than the synthetic surfactants in terms of adsorption, re-spreading, surface tension lowering capacity and film spreading. However, there is a slight more risk of intraventricular hemorrhage in case of the natural surfactants [15, 16].

Amongst the different constituents, cholesterol in SRT is highly disputed and hence, it drew our attention. Fig 3.1 shows the structure of cholesterol. It has been shown that cholesterol changes the

morphology of DPPC domains even at low concentrations [17]. However, Gunasekara et al., found that physiological amount of cholesterol has no effect on the surface activity on a natural surfactant BLES (Bovine Lipid Extract Surfactant) and only higher concentration imposes harmful effects on the behavior of lung surfactants [18]. Gomez-Gil et al., also showed that cholesterol and natural surfactant protein SP-C put together in physiological conditions may improve the surface activity of LS. [19] Moreover, Kim et al. recently showed that small amounts of cholesterol lower the surface viscosity of model DPPC monolayers, suggesting that addition of small amounts of cholesterol would be beneficial to the efficient spreading of synthetic LS in SRT [17] Therefore, in this chapter, we focused on understanding the molecular interactions between small and elevated amounts of cholesterol and synthetic surfactant protein MiniB in a simple binary phospholipid mixture, DPPC:POPG (7:3), that is often used as a model of LS mixtures containing saturated and unsaturated lipids as well as zwitterionic and anionic lipids. We particularly focus on the effects of cholesterol on the surface activity and domain morphology of these model LS films, in the presence and absence of MiniB.

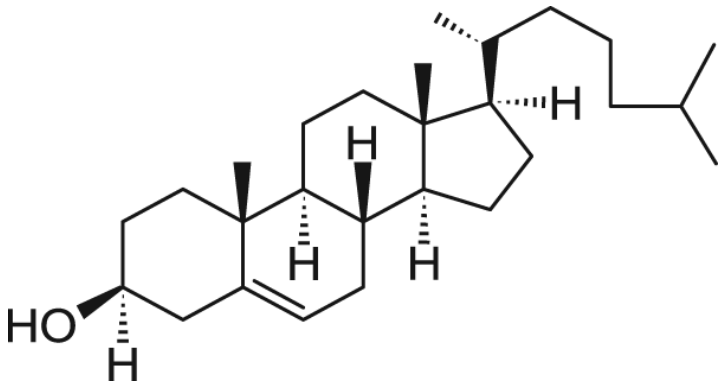

Fig 3.1: Structure of cholesterol (adapted from Avanti Polar Lipids).

Mini B is a 34 amino acid residue of the native lung surfactant protein SP-B, where the N and C terminals of the native protein are merged together [20, 21]. Fig 3.2 shows the structure of Mini B [20]. We are well aware of the functions of SP-B[22]. Removal of SP B gene (SP $B^{-/-}$) in mice was shown to cause fatal post-natal respiratory distress [23] and therefore, SP B is an invaluable component of LS. The development of a synthetic analog of SP-B is naturally of therapeutic importance as it overcomes the problem of bulk extraction and purification of the native protein. Studies such as that performed by Walther et al., showed that MiniB can aid an artificial surfactant, diether phosphonolipid (DEPN), in lowering surface tension efficiently [24]. It has also been previously reported that SP-B increases the line tension of the phospholipid domains at the air-water interface [25] and thus, Mini B must have similar propensity. On the other hand, cholesterol lowers the line tension [17] as can be evidenced by the stretching out of the domains. Therefore, Mini B and cholesterol have opposing effects on the lung surfactant phospholipids, which is why, we aimed at understanding how the two would behave in the same environment.

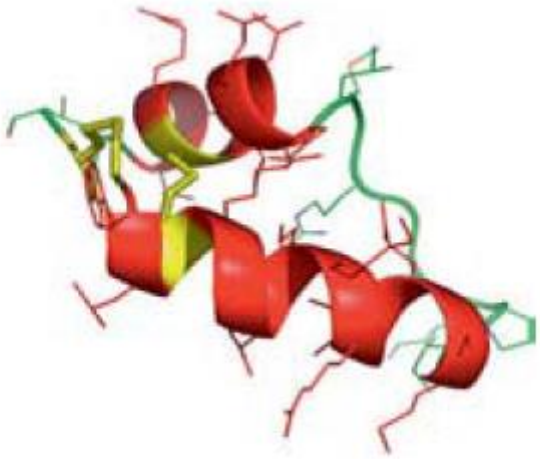

Fig 3.2: Structure of Mini B. The disulphide link between the N-terminal and C-terminal is given in yellow. This image was adapted from ref. 20.

3.3 Materials and Methods:

3.3.1 Materials: The lipids, 1,2-dipalmitoyl-*sn*-glycero-3-phosphocholine (DPPC), 1-palmitoyl-2-oleoyl-*sn*-glycero-3-phospho-(1'-*rac*-glycerol) (POPG) and cholesterol were purchased from Avanti Polar Lipids, Inc. (Alabaster, AL) in powder form for cholesterol and at final concentrations of either 25 mg/ml or 5 mg/ml in organic mixtures of chloroform for the others. The synthetic protein MiniB (a mimic of the native surfactant protein SPB) was generously provided by our collaborator, Dr. Alan J. Waring (Department of Medicine, Harbor-UCLA Medical Center, Torrance, Ca). Organic solvents, acetone, isopropanol and chloroform, were purchased from Thermo Fisher Scientific Inc. (Pittsburgh, PA). The fluorescent dye, 1, 2-Dihexadecanoyl-*sn*-Glycero-3-Phosphoethanolamine, Triethylammonium Salt (TXR-DHPE), was obtained from Life Technologies (Invitrogen, Grand Island, NY) in a dried form. The lipids were stored at -20 ^{o}C to prevent any evaporation of the organic mixture. Water which served as a sub-phase as well as cleaning agent was purified (resistivity of 18.2 MΩ cm) using Direct-Q 3 UV System purchased from EMD Millipore (Billerica, MA).

3.3.2 Methods: DPPC: POPG solutions were prepared in the ratio of 7:3 by weight as DPPC is the primary composition of LS. 1wt%TXR-DHPE dye was used for imaging purposes. Multiple compositions of MiniB and cholesterol along with DPPC and POPG were used which is reported in Table 1.

Table 3.1: The table summarizes the LS mixtures tested in this study. Numbers refer to the amount by weight of MiniB and cholesterol that was added to a mixture of DPPC: POPG (7:3).

DPPC: POPG (7:3)	Cholesterol (wt.)		
MiniB (wt.)	0,0	0,1	0,5
	1,0	1,1	1,5
	5,0	5,1	5,5

All the mixtures were diluted in chloroform. Samples were dried down with nitrogen for storage purposes in order to retain the activity of the protein.

A Langmuir trough (Biolin Scientific Inc.), with a moveable ribbon that is used to mimic the compression and expansion process in the alveoli was used such that the a maximum open area of the trough was 166 cm^2, while the minimum area was 46 cm^2. Samples were added drop wise with a Hamilton glass Syringe on an aqueous sub-phase and 20 minutes were given each time before running the experiment to allow the chloroform to evaporate. For isotherm experiments a compression rate of 125 cm^2/ min was chosen, however, for imaging purposes a slower, quasi-static, rate of 7 cm^2/ min was selected to ensure better focusing. Surface pressure was measured using Wilhelmy plate balance (filter paper). A Nikon Eclipse fluorescence microscope was used to visualize the lipid domain formation on the air-water interface. The images, at an interval of 1 to 5 mN/m in the different monolayer phases, were captured using CCD camera (Andor LUCA). 5 frames were used for each image sequence and representative imageswere selected for reporting purposes.

The domain morphology and size of the liquid condensed domains were analyzed with ImageJ (NIH) software. Two neighboring images were analyzed for each image sequence for better statistical quality. Graphs were generated using Origin 8.62 (OriginLab, Northampton, MA).

3.4 Theory:

3.4.1 Compressibility modulus: The compressibility of an interface is used to understand the mechanical properties of a monolayer. The two-dimensional isothermal bulk-modulus, β, calculated to understand a substance's ability to store energy in the form of stress, is given by the following equation:

$$\beta = -A\left(\frac{\partial \Pi}{\partial A}\right)_T = A\left(\frac{\partial \gamma}{\partial A}\right)_T = 1/\kappa \qquad (1)$$

Here, κ is the isothermal compressibility.

β, as well κ, are the second order derivative of Gibb's free free energy and any dip in the β vs. A curve implies a first order phase transition. From a compressibility modulus data we can comment on the packing of a monolayer and higher incompressibility is essential for the proper functionality of LS.

3.4.2 Condensed Area Fraction: The condensed area fraction is the ratio of the total condensed area, i.e., the dark domains found in the two-phase coexistence region and beyond, to the total area of the image. It provides us with an estimate of the fraction of the monolayer that has condensed at a given surface surface pressure. Mathematically, the percentage area fraction is:

$$\frac{\text{Total area of the Dark Region}}{\text{Total Area}} \times 100\ \% \qquad (2)$$

3.4.3 Determining line tension from domain size distribution: The shape of lipid domains in a monolayer depends on a balance between the electrostatic energy and the line tension. Based on this theory along with the minimization of free energy, the size distribution of the domains can be given by the following equation[25].

$$C_N = \left[C_M \exp\left[-\left(\frac{(\Delta m)^2 R_o (R_o/R - 1)^2}{4\varepsilon\varepsilon_o k_B T} \right) \right] \right]^{R^2/R_o^2} \quad (3)$$

Here, C_N and C_M are the fraction of domains. Δm is the dipole density, R_o is the radius corresponding to minimum energy, ε is the dielectric constant for interfacial water, ε_o is the permittivity of vacuum, k_B is the Boltzmann constant and T is the temperature. The parameters, CM, $(\Delta m)^2 R_o / 4\varepsilon\varepsilon_o k_B T$ and R_o are evaluated using a non-linear curve fit and then, the following equation [25], relating R_o with line tension (λ) and Δm, is used to determine the line tension of the lipid domains.

$$R_o = \frac{1}{\rho_o} = \left(\frac{e^3 \delta}{4} \right) \exp\left[\frac{[4\pi\varepsilon\varepsilon_o \lambda]}{(\Delta m)^2} \right] \quad (4)$$

3.5 Results:

3.5.1 Isotherms: Figure 3.3 presents the quasi-static surface pressure vs mean molecular area isotherms of the different samples examined. Each sample was tested thrice and the plots given here are the representative ones. Here, surface pressure is the difference between the surface tension of pure water and the surface tension of water containing surfactants. Mathematically,

$$\text{Surface Pressure, } \Pi = (\gamma_0 - \gamma) \quad (5)$$

Where γ_0 is the surface tension of pure water (72 mN/m) and γ is the surface tension of water with surfactant. As the area of the trough is reduced, surface tension of Langmuir monolayers decrease due to increased packing or the surface pressure of the Langmuir film increases .

Fig 3.3A shows how the isotherm of a mixture of DPPC:POPG was modified by varying the concentration of Mini B. The solid line represents the control curve for DPPC:POPG. At higher mean molecular areas, the monolayer was in a gaseous phase. However, with the decrease in area, the monolayer went through changes in phase and the molecules got more ordered. In case of the control, the coexistence of the liquid-expanded phase and the liquid-ordered phase was approximately between the surface pressure 15 mN/m and 30 mN/m. Beyond this point, there was a rapid rise in surface pressure with very little area compression and the monolayer finally collapsed at close to 72 mN/m. With the addition of 1 % Mini B to the system, we observed practically no change in the isotherm. This curve is given as dashed line and it almost overlaps with that of the control. However, when 5 % Mini B was added to DPPC:POPG, given by the dotted line, the isotherm got shifted to higher values of surface pressure at any given mean molecular area. This suggests that with the inclusion of higher amount of Mini B, there is an ease in the lowering of surface tension.

Fig 3.3B represents the effect of addition of varying amounts of cholesterol on the isotherm of DPPC:POPG. With the addition of 1% cholesterol, given by dash dot curve, there was no significant change in the isotherm. However, there was a shift of the isotherm to lower values of mean molecular area at the higher pressures corresponding to collapse region. With the addition of 5% cholesterol to DPPC:POPG, isotherm deviated even further towards the lower area values suggesting greater changes in the mechanical properties at the collapse. Other than that, the slope of the liquid-condensed region was shifted to slightly higher mean molecular areas.

Fig 3.3C is a plot of DPPC:POPG mixed with 1 % MiniB and varying composition of cholesterol. This plot shows how 1% of the artificial surfactant protein interacts with multiple concentrations of cholesterol.

The isotherm for MiniB 1 % and cholesterol 1 % is shown by the dashed curve. Here, we could observe that the isotherm was pushed to higher values of surface pressure for the same mean molecular area. This again suggests an improvement in the surface tension lowering capabilities of the surfactant. Next, the concentration of cholesterol was raised to 5 % and the curve (dotted lines) fell back close to the control.

Fig 3.3D represents the effect of 5 % Mini B with cholesterol on DPPC:POPG. 1 % cholesterol, given by dashed line, overlapped with the control till the two phase coexistence region of the isotherm. Beyond this, the slope for the condensed region was lower than that of the control. This indicates that this mixture is not as efficient as the control in lowering surface tension. The effect was more pronounced with 5 % Mini B and 5 % cholesterol as can be seen from the thin dashed curve. The isotherm moved further to the left of the control indicating the need for higher area compression to achieve the same values of surface pressure.

3.5.2 Compressibility Modulus: Fig 3.4 presents the compressibility modulus as a function of mean molecular area of the samples tested. The data was processed using an FFT filter over 5 points.

Fig 3.4A shows the compressibility modulus for varying composition of Mini B with DPPC:POPG. In case of the control, the compressibility modulus gradually increased till it reached around 30 mN/m and after this, there was a slight dip in the curve. At around 45 mN/m there was again a rise in the compressibility modulus with the peak touching a value of 70 mN/m, beyond which, there was a sharp fall. In case of 1 % Mini B, presented as dashed lines, there was almost no change, till a slight decrease in the values for the second peak was observed. 5 % Mini B on DPPC:POPG was more compressible at lower mean molecular areas. But, it almost overlapped with the control when the mean molecular area was reduced to approximately 45 mN/m. The second peak in this case was lower than control suggesting reduced compressibility i.e., less packing.

Fig 3.4B shows the effect of different concentration of cholesterol on the compressibility modulus of DPPC:POPG. With 1 % cholesterol, there was a lowering of the compressibility of the system at low mean molecular area. There was a slight shift of the peak towards higher area. However, with 5 % cholesterol, there was appreciable change in the compressibility data at areas lower than 60 $Å^2$/ molecule. The maximum compressibility dropped and moved even further towards lower areas.

Fig 3.4C gives the compressibility modulus for systems containing both Mini B and cholesterol. With Mini B 1 % and cholesterol 1 % (dashed curve), there was an increase in the compressibility of the system. This suggested a change in the domain morphology at the air-water interface. In case of 1 % Mini B and 5 % cholesterol (dotted line), the curve shifted to the left and the peak was nearly the same as that for the control.

Fig 3.4D represents the compressibility modulus of DPPC:POPG along with 5 % Mini B and varying concentration of cholesterol. Here, we found appreciable deviation from the control. The slope at area lower than 50 $Å^2$/ molecule was more gradual than the control and at higher compression, the value of the peak was lower. The same changes were even more prominent for Mini B 5 % and cholesterol 5 %.

3.5.3 Flourescence Images: To have a better understanding of the changes occurring at the monolayer, we performed fluorescence microscopy to monitor changes in the monolayer domain morphology and size. Images were recorded throughout the monolayer compression cycle at intervals of 5 mN/m. However, we present here images at surface pressures 20 mN/m, 30 mN/m (Fig 3.5) and at monolayer collapse (Fig 3.6) for simplicity. At 20 mN/m, the monolayer has two phases, namely the liquid expanded (LE) and the liquid condensed (LC) phases, coexisting simultaneously for DPPC:POPG and 30 mN/m marks the upper boundary for this phase-coexistence region. Beyond thissurface pressure, the samples get densely packed. At the highest values of surface pressure, (coinciding with lowest values of surface tension) we visualize cracks and “folds” on the surface of the monolayer. These features mark the

transition of material from a two-diensional film to the three-dimensional bulk phase. Such features appear in the monolayer since material is squeezed out of the monolayer due to excessive compression.

3.5.3.1 Phospholipid monolayer domain morphology: Fig 3.5A and 3.5D shows the images for DPPC:POPG (7:3) at surface pressures 20mN/m and 30 mN/m respectively. Contrast in these images is due to the selective segregation of the dye molecules. The dark regions are the condensed domains where the bulky dye molecules cannot insert themselves, whereas the lighter region is in liquid-expanded phase allowing the dye to blend in. In case of the control, the monolayer was found to be well packed beyond a surface pressure of 20 mN/m, agreeing with previously reported results [26]. The domains were more or less circular in shape. Fig 3.5B and Fig 3.5E shows the images for DPPC:POPG (7:3) with 1 wt. % cholesterol added to the system. Here we observed a drastic change in the domain morphology. The domains stretched out and in place of the circular condensed regions, we found protruding spirals along the boundaries. The effect became more pronounced with the rise in the surface pressure. Fig 3.5C and 3.5F shows the effect of adding 5 % cholesterol to a DPPC:POPG mixed lipid system. In this case, the domains were even more stretched out. Moreover, the packing density of liquid condensed domains decreased significantly. Next, we monitored the effect of 1% Mini B on DPPC:POPG (Fig 3.5G and 3.5J). The shapes were similar to the control as can be seen in the images. Fig 3.5H and 3.5K had 1 % Mini B and 1 % cholesterol in the system. Here, the edges did not modify. Although, the domains were no longer round in shape, yet, Mini B did not allow cholesterol to completely dominate the domain formation. The domains got curled up in this case. With 1 % Mini B and 5 % cholesterol (Fig 3.5I and Fig 3.5L) the domains were completely transformed without getting packed at all. Images 3.5M and 3.5P show the effect of 5 % Mini B. Here, the domains appeared less packed and smaller in size. However, the shape remained the same. Fig 3.5N and Fig 3.5Q shows the effect of 1 % cholesterol along with 5 % Mini B. There were no appreciable changes in the shape of the domains and Mini B dominated over the presence of cholesterol. Finally, we

monitored phospholipid films containing 5 % Mini B with the same concentration of cholesterol added to DPPC:POPG. In these monolayers,the size of the domains was found to be smaller. However, cholesterol could not modify the shape of the domains. The monolayer was much less packed.

3.5.3.2 Collapse: When LS monolayer is compressed, the unsaturated lipids, which cannot sustain high pressure, squeezes out of the monolayer. Thus, a transition from 2D monolayer to a 3D multilayer occurs. This is termed as the collapse and Fig 3.6 shows the images that were taken after the surfactant films had collapsed. Such a collapse is due to buckling of the film rather than fracture or solubilization. In case of fracture or solubilization, there is a loss in the material from the surface as these squeezed out materials cannot be reincorporated into the monolayer with subsequent compression expansion cycles [27]. Thus, in those cases, the materials collapse irreversibly, and appear as bright dots on the air-water surface. Large bright fold-like regions on the monolayer are indicative of reversible collapse with lower loss of material. These bright regions resembling cracks on the surface can be compared to that formed by folding a piece of paper and can be visualized in Fig 3.6A in case of the DPPC:POPG controlled system. When cholesterol is incorporated into the system (Fig 3.6B for 1 %and 3.6C for 5 %), this crack across the monolayer, disappears and instead bright dots, begin to appear at the surface. This suggests that cholesterol hinders the retention of lung surfactant material near the surface. On the contrary, when MiniB is added to the system, there is an increase in the collapse crack, both for 1 % and for 5 %. Fig 3.6D and 3.6G shows the formation of thick collapse cracks in case of 1 % and 5 % respectively. Fig 3.6E shows the effect of 1 % cholesterol and 1 % Mini B on DPPC:POPG. The lines still form in this case indicating that even higher surface pressures, Mini B does not allow cholesterol to completely dominate over the behavior of the system. However, with 5 % cholesterol and 1 % MiniB (Fig 3.6F), there was hardly any bright region on the surface. Fig 3.6H shows the effect of 1 % cholesterol and 5 % Mini B. Here we can again find substantial amount of crack on the surface, indicating the dominance of higher weightage of Mini B over cholesterol.

Finally, 5 % of both the components showed a large number of dots on the surface. The cracks appeared similar to the ones formed by folding cardboard instead of a paper.

3.5.4 Percentage Condensed Region: Fig 3.7 shows the percentage of the monolayer that formed Liquid-Condensed region. The amount of condensed region may contribute to the fluidity of the monolayer. Surface pressures 15, 20, 25 and 30 mN/m were chosen as they represent the two phase region. Fig 3.7A shows the effect of cholesterol on DPPC:POPG. The condensed domain increased from 50% to 60% as a function of SP in case of the control system. However, with cholesterol, there was a reduction in the total area of condensed domains. The effect was more pronounced in monolayer films containing higher concentrations of cholesterol. Fig 3.7B shows how Mini B alters the formation of condensed domains in DPPC:POPG. With 1% Mini B, there was lowering in the domains till 20 mN/m surface pressure, however, at 25 and 30 mN/m, there was an increase. But with 5% Mini B there was a drop in the condensed domains throughout. The next two figures reveal how Mini B and cholesterol both act together in altering the area of the dark domains. In Fig 3.7C the composition of Mini B was fixed at 1% and cholesterol was varied. Here again, with 1% of both put together there was increase in the domain area at 25 and 30 mN/m. but, 5% cholesterol dominated over 1% Mini B. There was a significant drop in the condensed domain in this case. Fig 3.7D shows the effect of varying amount of cholesterol on 5% Mini B. In this case, 5% Mini B dominated over cholesterol, however at equal concentration of the two components, the area reduced drastically. This showed the dominance of higher concentration of cholesterol even with equal amount of Mini B.

3.5.5 Line Tension: The model to calculate the line tension used here is only feasible for lipid domains that are circular in shape. So we were limited to measuring line tension of the domains for the control, lipid mixture with both 1% and 5% Mini B and the mixtures that had 5% Mini B and varying concentration of cholesterol. Surface pressures 15 mN/m and 20 mN/m were selected for the ease of analysis. Beyond this

pressure, the monolayer gets relatively more packed, making it hard to analyze. The line tension of the control (Fig 3.8A) was around 3 x 10^{-2} pN at 15 mN/m and this value dropped to 2.4 x 10^{-2} pN. However, with the addition of MiniB, there was a rise in the line tension. Also, in this case, there was an increase in line tension with surface pressure. With 1% Mini B, line tension was around 4.5 x 10^{-2} pN at 15 mN/m and 5 x 10^{-2} pN at 20 mN/m. 5% Mini B showed values slightly higher than those for 1%. When 1% cholesterol was added to 5% Mini B (Fig 3.8B), there was a rise even though cholesterol on its own is known to reduce line tension. However, when 5% cholesterol was added instead of 1%, there was a drop in line tension revealing the dominance of cholesterol over Mini B in this case.

3.6 Discussion:

This work is inspired by the viability of Mini B to act as a surfactant protein in SRT. Also, cholesterol is a highly debated component of the LS and majority of the LS mixtures in SRT avoid cholesterol. Previous work has shown the harmful effects of cholesterol on LS mixtures [28, 29]. However, we wanted to observe whether Mini B can play a role in countering the effects of cholesterol on LS. We used a simple LS mixture, DPPC:POPG mixed in the weight ratio of 7:3, to understand the above interaction. This ratio was selected because DPPC forms the main component of LS, whereas POPG is representative of the anionic lipids found in LS, and this composition is used as a standard mixture in biophysical studies related to this area of research. We obtained surface pressure-mean molecular area isotherms to determine whether these two components alter the capability of the lipid mixture to lower surface tension, which is the primary function of LS. From this, we also looked into the changes in the mechanical properties of the system by deriving the compressibility modulus. Finally, we scrutinized them under the microscope to visualize the changes in the phospholipid domain formation in the presence of Mini B and cholesterol, both individually as well as put together. Our results show that lower amount of Mini B as well as cholesterol (1 %) enhances the properties of LS. However, high concentration of Mini B and cholesterol (5

%) put together plays a negative role. The domains, as seen previously [30], changes drastically in the presence of cholesterol and the effect is, to a certain extent, countered by Mini B. We will discuss the results in more details in the following sub-sections.

3.6.1 Effect on Mechanical Properties: The surfactant mixture DPPC:POPG is efficient in lowering surface tension to near zero values owing to the presence of the disaturated phospholipid which has been reported previously[31]. A low concentration of Mini B does not alter this property at all. However higher concentration introduced an early condensation in the lipid mixture at the air-water interface. On the other hand, we found changes only in the collapse pressures in case of cholesterol while at lower pressures there was practically no change in the surface tension lowering abilities with the concentrations tested. Next, we tried a combination of both the components and we noted appreciable changes in this case. A lower concentration of both the components showed an improvement. However, equal amounts of both at higher concentration had detrimental effects on the LS. The surface tension in this case fell short of the zero mark. Even when the concentration of Mini B was higher than that of cholesterol, LS failed to put up a good performance. This suggests that beyond a certain concentration of the two put together, there is an adverse effect.

Compressibility modulus of the system can be derived directly from the pressure vs. area curve[32]. The compressibility of the system lowers in the presence of cholesterol, however, Mini B does not have an appreciable effect on the fluidity of the system. When the two are put together in equal but low concentration, there is an increase in the compressibility of the system. A higher concentration of the two, on the other hand, showed significant fluidization in the system which proved to be unfavorable for achieving low surface tension.

From the above data we concluded that a low concentration of both Mini B and cholesterol may aid LS in carrying out its desired function. We then looked into the lipid domains in more details to have a better understanding of the system.

3.6.2 Tug of war: Effect on Lipid Domain Formation: DPPC:POPG forms almost circular domains at the air-water interface[26]. By 20 mN/m surface pressure, the domains get very well packed owing to the presence of high percentage of DPPC. At surface pressures close to 70 mN/m, DPPC:POPG collapses reversibly. This was apparent because of the presence of the bright folded region in the monolayer. At lower surface pressures, Mini B reduces the packing density of the domains. However, it causes no change in the domain structure of DPPC:POPG. At higher surface pressures giant folds are formed which suggests Mini B, like SP B [33], helps in holding the surfactants near the surface. Therefore, Mini B allows the subsequent cycles of compression and expansion to reutilize the unsaturated lipids, preventing loss due to squeeze-out. Cholesterol, on the other hand, shows a very opposing effect on DPPC:POPG. The domains stretch out and the effect becomes more pronounced as the concentration of cholesterol is increased. It significantly lowers the packing as well. Although the changes were subtle in case of the isotherms, as we took a closer look, the film was much more fluid in presence of cholesterol. At higher surface pressure cholesterol prevents the formation of collapse cracks. Instead, solubilization occurs and materials get lost to the subphase. However, there is a tug of war when Mini B and cholesterol are both present together. Mini B tries to keep the domains circular whereas cholesterol wants to stretch it apart. At uneven concentration, either Mini B or cholesterol dominates depending on which one has the higher weight. This is true at both lower end as well as the upper end of the surface pressure-area isotherm. However,1% of both the components put together, reveals that even though cholesterol tries to stretch out the domains to lower line tension, the change is not as drastic as that can be seen only in case of cholesterol. There was an increase in the area of the condensed domain at higher pressures as can be seen in Fig 3.7C. The presence of cholesterol did not adversely affect the mechanisms of reversible collapse. When 5% of both Mini B and cholesterol were added to the system, there was no change in the shape of the domain but the domains size was reduced. Fig 3.7D clearly shows the decrease in the percentage condensed

domain when higher concentration of both was used. Here again, at collapse, solubilization of the material was more predominant.

Therefore, the images show a balance of the substances at lower concentration and a lower concentration of the two components put together is favorable.

3.6.3 Effect on Line Tension: Line tension between the domains contributes to the viscoelasticity of the monolayer at the air-water interface. This viscoelasticity controls the spreading and rate of collapse of the monolayers [25]. More viscous properties are needed for the material to spread uniformly along the entire surface, however, the monolayers should be elastic enough to fold under high compression and get readsorbed quickly to the interface with subsequent expansion. Cholesterol reduces the line tension of the phospholipid domains, which causes lipids to stretch out. However, Mini B helps in increasing the line tension of the domains. Fig 3.8A revealed this rise in line tension with the addition of Mini B. The model we used is applicable only for circular domains. Therefore, when cholesterol and Mini B both were added to the system, only the data for 5% Mini B and varying concentration of cholesterol could be analyzed. At both 15 mN/m and 20 mN/m, there was an increase in the line tension when the composition of cholesterol was lower than that of Mini B. However, with 5% of both the components, there was a decrease in the line tension value.

Therefore, both percentage condensed domain and line tension analysis revealed the disadvantage of using cholesterol and Mini B together at higher concentration. However, a smaller amount of the two can definitely benefit LS.

3.7 Conclusion:

The research reported here puts forward the opposing effects of the synthetic LS protein Mini B and the much debated cholesterol at the air-water interface on the quasi-equilibrium state of the phospholipid domain morphology. We observed that Mini B alone serves the important purpose of keeping much of the LS components from being lost into the sub-phase as the monolayer is compressed. It also increases the line tension of the domains, which in turn maintains the stability of the domains. Cholesterol, on the other hand, increases the fluidity of the lipid but drastically transforms their shapes as well as makes the lipids collapse irreversibly. A high concentration of cholesterol, as already mentioned in the literature, is not advisable and may even result in ARDS. However, the two components together even out the opposing forces, and a competitive synthetic composition of LS for SRT is possible. From our studies we conclude that low concentration of cholesterol and Mini B together can help in achieving the desired high surface pressure while keeping the film adequately fluid along with collapsing reversibly with thick cracks. The inclusion of Mini B into the system can be advantageous as it is purely synthetic and therefore the yield will be much higher than using the natural counterpart. Addition of cholesterol is needed as it makes the lipid mixture more dynamic and it is a part of the natural surfactant. Our report therefore, provides the evidence that it is possible to include both Mini B and cholesterol.

3.8 Figures:

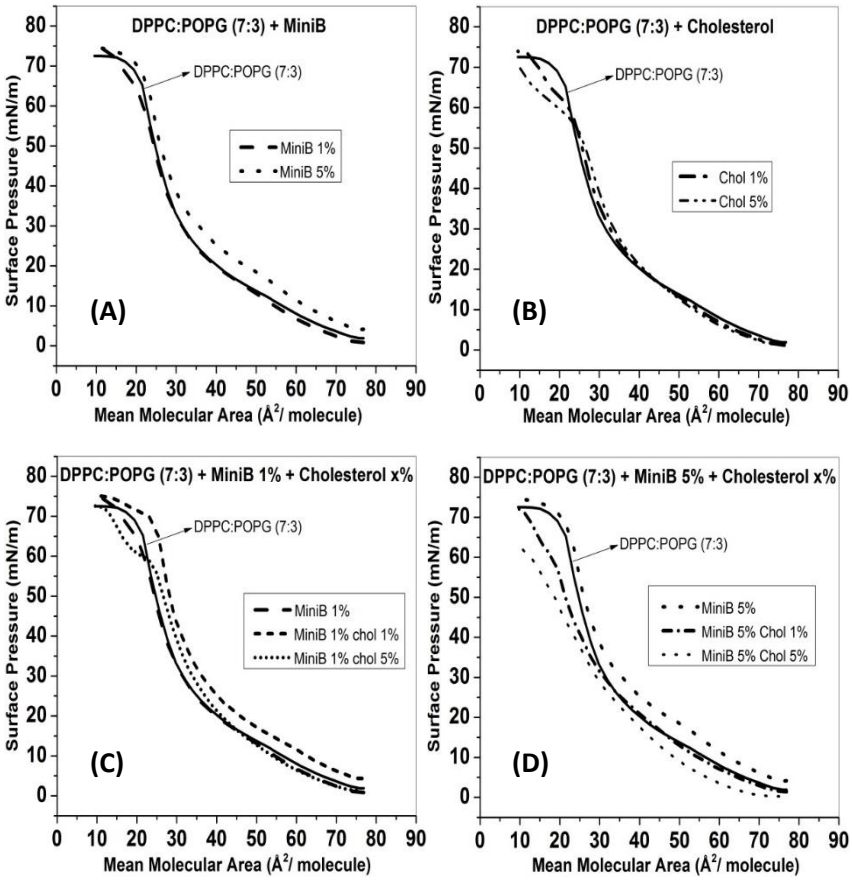

<u>Fig 3.3:</u> Surface pressure vs. mean molecular area isotherms for different lung surfactant mixtures. (A) DPPC:POPG (7:3) with 1% and 5% MiniB. (B) DPPC:POPG with 1% and 5% cholesterol. (C) DPPC:POPG with 1% MiniB and varying concentration of cholesterol (D) DPPC:POPG with 5% MiniB and different weightage of cholesterol. The isotherms indicate an improvement in surface tension lowering abilities with 1% of both Mini B and cholesterol in the mixture.

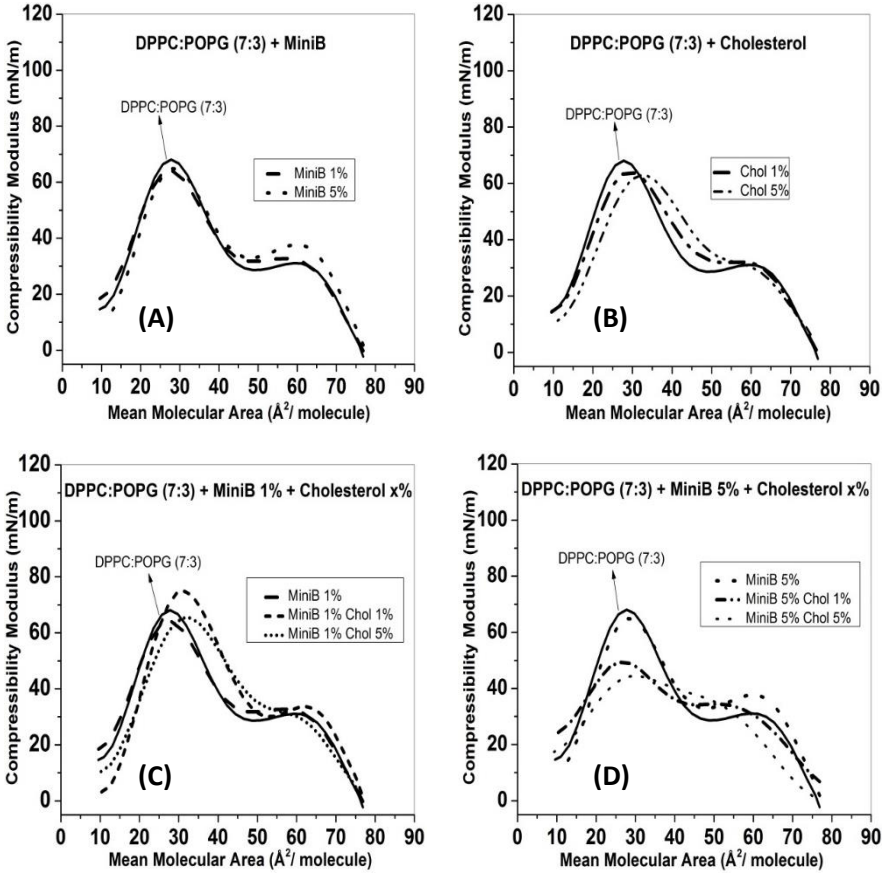

Fig 3.4: Compressibility Modulus for different lung surfactant mixtures. (A) DPPC:POPG (7:3) with 1% and 5% MiniB. (B) DPPC:POPG with 1% and 5% cholesterol. (C) DPPC:POPG with fixed MiniB percentage (1%) and varying weightage of cholesterol (D) DPPC:POPG with 5% MiniB and different amounts of cholesterol. Higher concentration of MiniB and cholesterol makes the monolayer more compressible whereas lower concentration of the increases the compressibility. An increase in compressibility modulus implies more packing and is therefore, favorable.

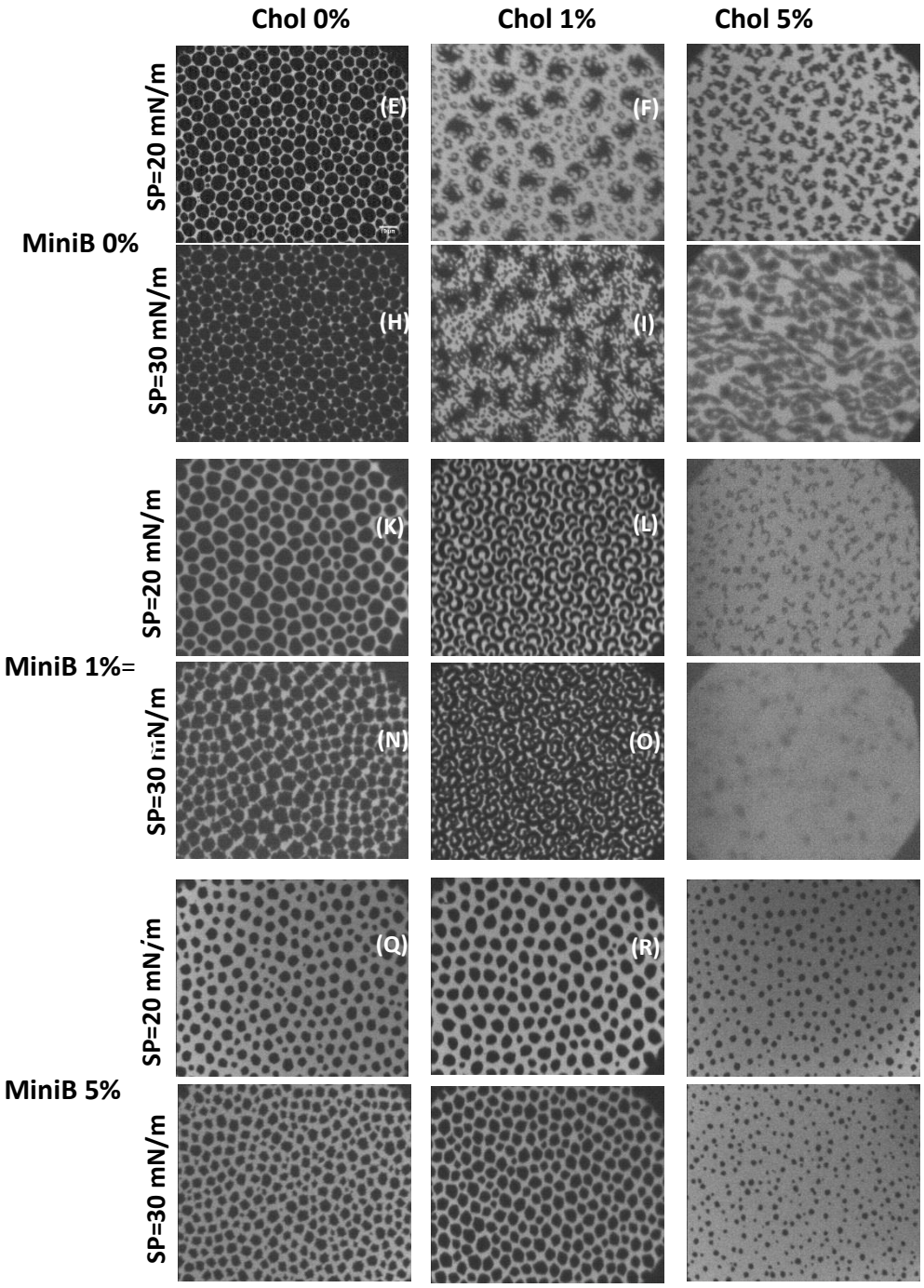

Fig 3.5: Fluorescence images of DPPC:POPG (7:3) along with MiniB and cholesterol in varying concentrations. Images A, B, C, G, H, I, M, N, O, P, Q and R were taken at 20 mN/m which lies in the two-phase coexistence region and the rest were taken at 30 mN/m which marks the upper boundary for the same region. Beyond this point, the domains get highly packed for the control. The first two rows are for samples without MiniB, the next couple rows are for samples with 1% MiniB in them, and the last two are

for ones with 5% MiniB. Concentration of cholesterol increases from left to right. The images reveal the inherent tendency of cholesterol to stretch out domains whereas, the MiniB showed opposite characteristics.

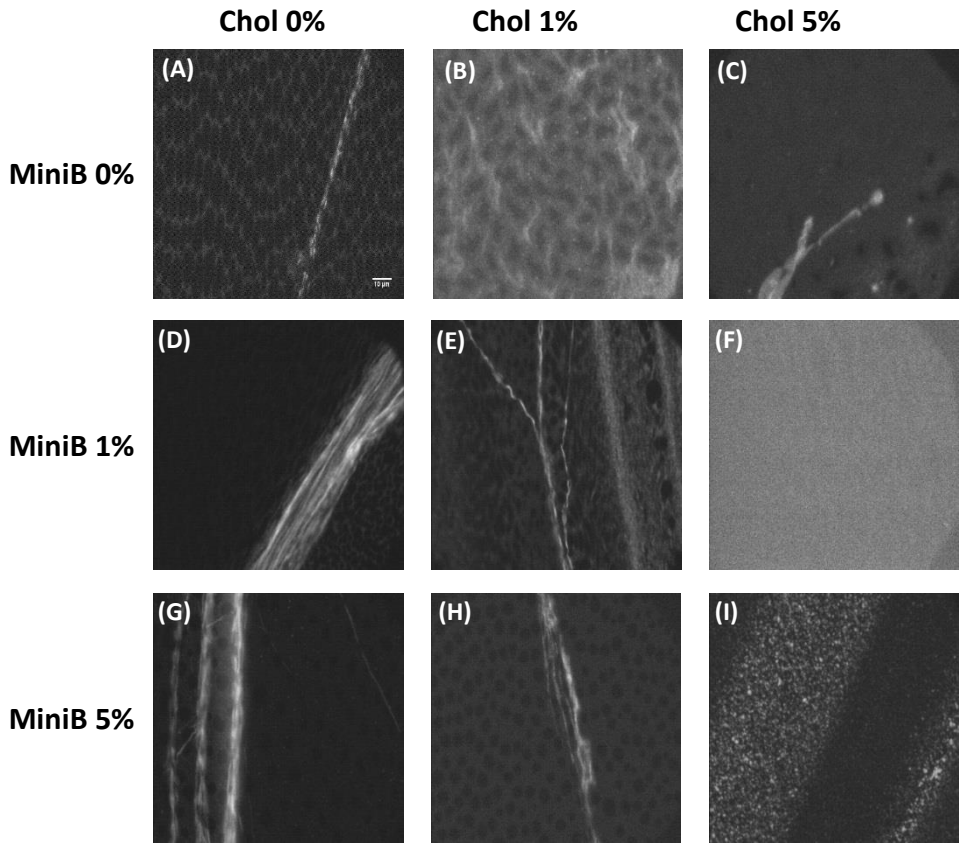

Fig 3.6: Fluoresecence images of DPPC:POPG(7:3) with different concentrations of MiniB and cholesterol after collapse. Concentration of MiniB changes columnwise whereas, the concentration of cholesterol changes along a row. MiniB produces thick cracks (D and G) upon collapse but cholesterol collapses irreversibly (B and C). With both put together, cracks can still be observed in case of 1% MiniB with 1% cholesterol (E) or 5% MiniB with 1% cholesterol (H). However, cholesterol dominates at higher concentration (F and I). DPPC:POPG on its own produces thin collapse cracks (A).

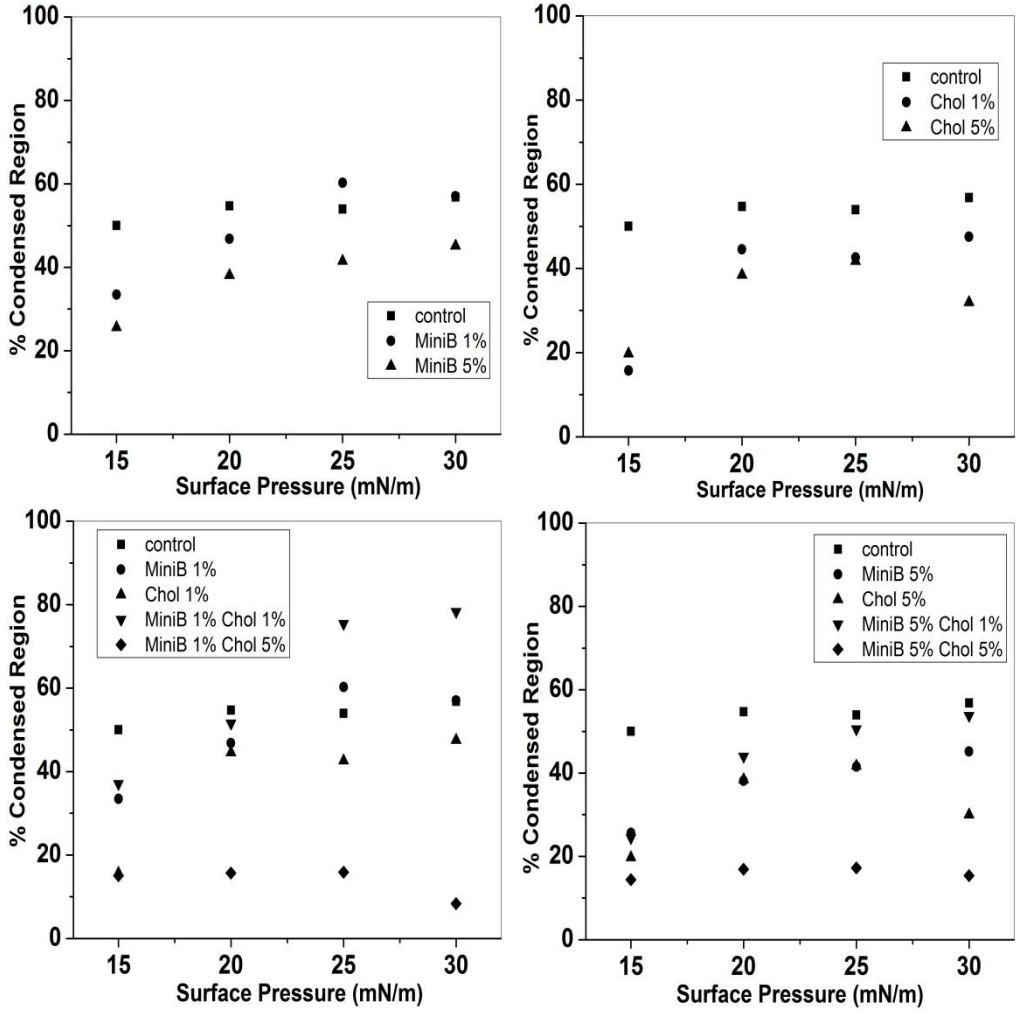

Fig 3.7: Percentage condensed domains for varying mixtures of DPPC:POPG (7:3). Percentage condensed domains show the amount of area that has condensed in the two-phase coexistence region. (A) Effect of MiniB on DPPC:POPG has been shown here. A reduction in the area was noted for 5% MiniB. (B) cholesterol reduces the area and the effect is more pronounced with an increase in choleserol concentration. (C) Interaction of 1% MiniB with different concentrations of cholesterol has been shown in this graph. Interestingly, 1% MiniB along with 1% cholesterol (inverted triangle) increases the area of the condensed domains. (D) 5% MiniB along with different concentrations of cholesterol showed a decrease in area everytime.

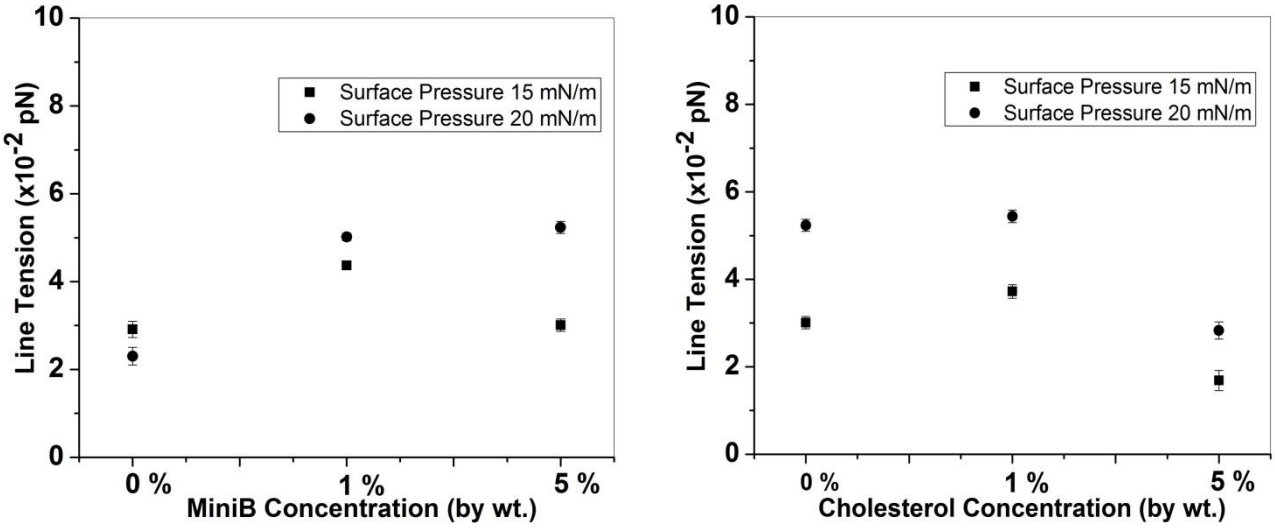

Fig 3.8: Changes in line tension for different mixtures. (A) MiniB increases the line tension between the domains (B) We could only measure the line tension for 5% MiniB with 1% cholesterol and 5% MiniB with 5% cholesterol as these domains were circular in shape. 1% MiniB with 1% cholesterol did not lower the line tension whereas, 5% of both revealed a lowering in line tension.

3.9 References

1. Robertson, B., J. Johansson, and T. Curstedt, *Synthetic surfactants to treat neonatal lung disease.* Molecular Medicine Today, 2000. **6**(3): p. 119-124.
2. Zasadzinski, J.A., et al., *The physics and physiology of lung surfactants.* Current Opinion in Colloid & Interface Science, 2001. **6**(5–6): p. 506-513.
3. Dohm, M.T., et al., *Biophysical Mimicry of Lung Surfactant Protein B by Random Nylon-3 Copolymers.* Journal of the American Chemical Society, 2010. **132**(23): p. 7957-7967.
4. Zuo, Y.Y., et al., *Current perspectives in pulmonary surfactant — Inhibition, enhancement and evaluation.* Biochimica et Biophysica Acta (BBA) - Biomembranes, 2008. **1778**(10): p. 1947-1977.
5. Clements, J. and M. Avery, *Lung Surfactant and Neonatal Respiratory Distress Syndrome.* American Journal of Respiratory and Critical Care Medicine, 1998. **157**(4): p. S59-S66.
6. K. Raghavendran, D.W., RH Notter, *Surfactant Therapy of ALI and ARDS.* Critical Care Clinics, 2011. **27**(3): p. 525-559.
7. Pérez-Gil, J., *Structure of pulmonary surfactant membranes and films: The role of proteins and lipid–protein interactions.* Biochimica et Biophysica Acta (BBA) - Biomembranes, 2008. **1778**(7–8): p. 1676-1695.
8. Parra, E. and J. Pérez-Gil, *Composition, structure and mechanical properties define performance of pulmonary surfactant membranes and films.* Chemistry and Physics of Lipids, (0).
9. Veldhuizen, E.J.A., et al., *The Role of Surfactant Proteins in DPPC Enrichment of Surface Films.* Biophysical Journal, 2000. **79**(6): p. 3164-3171.
10. Veldhuizen, R., et al., *The role of lipids in pulmonary surfactant.* Biochimica et Biophysica Acta (BBA) - Molecular Basis of Disease, 1998. **1408**(2–3): p. 90-108.

11. Keough, B.D.F.a.K.M.W., *Surface respreading after collapse of monolayers containing major lipids of pulmonary surfactant.* Chemistry and Physics of Liplds, 1988. **49**(1-2): p. 81-86.

12. Gómez-Gil, L., J. Pérez-Gil, and E. Goormaghtigh, *Cholesterol modulates the exposure and orientation of pulmonary surfactant protein SP-C in model surfactant membranes.* Biochimica et Biophysica Acta (BBA) - Biomembranes, 2009. **1788**(9): p. 1907-1915.

13. Wright, J.R., *Immunomodulatory functions of surfactant*. Vol. 77. 1997. 931-962.

14. Stevens, T.P. and R.A. Sinkin, *SUrfactant replacement therapy*.* Chest, 2007. **131**(5): p. 1577-1582.

15. Suresh, G.K. and R.F. Soll, *Lung Surfactants for Neonatal Respiratory Distress Syndrome: Animal-Derived or Synthetic Agents?* Pediatric Drugs, 2002. **4**(8): p. 485-492.

16. Soll Roger, B.F., *Natural surfactant extract versus synthetic surfactant for neonatal respiratory distress syndrome.* 2001(2).

17. KyuHan Kim, S.Q.C., Zachary A. Zell, Todd M. Squires, Joseph A. Zasadzinski, *Effect of cholesterol nanodomains on monolayer morphology and dynamics.* Proc Natl Acad Sci U S A, 2013 **110**(33): p. 3054-3060.

18. Gunasekara, L., et al., *Pulmonary surfactant function is abolished by an elevated proportion of cholesterol.* Biochimica et Biophysica Acta (BBA) - Molecular and Cell Biology of Lipids, 2005. **1737**(1): p. 27-35.

19. Gómez-Gil, L., Pulmonary Surfactant Protein SP-C Counteracts the Deleterious Effects of Cholesterol on the Activity of Surfactant Films under Physiologically Relevant Compression-Expansion Dynamics. Biophysical journal, 2009. **97**(10): p. 2736-2745.

20. Walther, F.J., Waring, A. J., Sherman, M. A., Zasadzinski, J. A., & Gordon, L. M., *Hydrophobic surfactant proteins and their analogues.* Neonatology, 2007. **91**(4): p. 303-10.

21. Walther, F.J., et al., *Critical Structural and Functional Roles for the N-Terminal Insertion Sequence in Surfactant Protein B Analogs.* PLoS ONE, 2010. **5**(1): p. e8672.21. Baoukina, S. and D.P.

Tieleman, *Lung Surfactant Protein SP-B Promotes Formation of Bilayer Reservoirs from Monolayer and Lipid Transfer between the Interface and Subphase.* Biophysical Journal, 2011. **100**(7): p. 1678-1687.

22. Baoukina, S. and D.P. Tieleman, Lung Surfactant Protein SP-B Promotes Formation of BilayerReservoirs from Monolayer and Lipid Transfer between the Interface and Subphase. Biophysical Journal, 2011. 100(7): p. 1678-1687.

23. Clark, J. C., et al., *TARGETED DISRUPTION OF THE SURFACTANT PROTEIN-B GENE DISRUPTS SURFACTANT HOMEOSTASIS, CAUSING RESPIRATORY-FAILURE IN NEWBORN MICE*. Proceedings of the National Academy of Sciences – PNAS, 1995. **92**(17): p. 7794- 7798.

24. Walther, F.J., et al., *Dynamic Surface Activity of a Fully Synthetic Phospholipase-Resistant Lipid/Peptide Lung Surfactant.* PLoS ONE, 2007. **2**(10): p. e1039.

25. Dhar, P., et al., *Lipid-Protein Interactions Alter Line Tensions and Domain Size Distributions in Lung Surfactant Monolayers.* Biophysical Journal, 2012. **102**(1): p. 56-65.

26. Pocivavsek, L., et al., *Lateral stress relaxation and collapse in lipid monolayers.* Soft Matter, 2008. **4**(10): p. 2019-2029.

27. Leonenko, Z., et al., *An Elevated Level of Cholesterol Impairs Self-Assembly of Pulmonary Surfactant into a Functional Film.* Biophysical Journal, 2007. **93**(2): p. 674-683.

28. Lee, K.Y.C., *Collapse mechanisms of Langmuir monolayers.* Annual review of physical chemistry. 2008. **59**: p. 771 – 791.

29. Hane, F., E. Drolle, and Z. Leonenko, *Effect of cholesterol and amyloid-β peptide on structure and function of mixed-lipid films and pulmonary surfactant BLES: an atomic force microscopy study.* Nanomedicine: Nanotechnology, Biology and Medicine, 2010. **6**(6): p. 808-814.

30. Malcharek, S., et al., *Multilayer Structures in Lipid Monolayer Films Containing Surfactant Protein C: Effects of Cholesterol and POPE.* Biophysical Journal, 2005. **88**(4): p. 2638-2649.

31. H. Diamant1(∗), T.A.W., 2, A. Gopal 3 and K. Y. C. Lee 3, *Unstable topography of biphasic surfactant monolayers.* Europhysics letters, 2000. **52**(2): p. 171 - 177.

32. Dwivedi, Mridula V., et al., *Size Influences the Effect of Hydrophobic Nanoparticles on Lung Surfactant Model Systems.* Biophysical Journal, 2014. **106**(1): p. 289-298.

33. Takamoto, D.Y., et al., *Interaction of Lung Surfactant Proteins with Anionic Phospholipids.* Biophysical Journal, 2001. **81**(1): p. 153-169.

Summary

The first chapter deals with the interaction of LS with anionic Engineered Carbon Nanodiamonds [ECN], a carbon based nanoparticle capable of serving as a carrier for drug delivery by inhalation. To assess the bio-toxicity of any nanoparticle, research so far has focused on changing the characteristics of those particles without stressing on the importance of the lipid mixture under concern. However, based on Surface pressure-area isotherms and Fluorescence Microscopy at an air-water interface, along with Atomic Force Microscopy, we reveal that this interaction is also modulated by the lipid head-group charge and alkyl chain saturation. Our study shows that ECN alters the shape of the phospholipid domains in the presence of zwitterionic lipids, but, in case of lipid mixtures containing anionic lipids, the negatively charged ECN lowers the packing density without modifying the shape of the domains.

The subsequent chapter focuses on understanding the interaction between MiniB, a synthetic analog of the natural surfactant protein SPB, and cholesterol, whose purpose and use is highly debated in SRT, in the presence of a simple binary mixture of LS phospholipids, namely, 1,2-dipalmitoyl-*sn*-glycero-3-phosphocholine (DPPC) and 1-palmitoyl-2-oleoyl-*sn*-glycero-3-phospho-(1'-*rac*-glycerol) (POPG). This study was undertaken as there is yet to be a consensus on the composition of LS used in SRT, especially the interaction between the various components of the mixture. Based on surface pressure-area isotherms and fluorescence imaging under constant compression, we conclude that a low concentration of Mini B along with an equal concentration of cholesterol aids in the proper functioning of synthetic LS. cholesterol prefers to stretch out the phospholipid domains by lowering line tension and also makes LS collapse irreversibly. On the contrary, a domain size distribution analysis reveals that Mini B increases line tension between the domains. Mini B also helps LS to collapse reversibly forming giant folds, therefore, preventing material loss from the interface. A tug of war ensues as the two are put together and Mini B dominates at lower concentrations of the two. However, at higher concentration, cholesterol tends to be the dominating component.

Conclusion and Future Directions

The study involving the interaction of Engineered Carbon Nanodiamonds [ECN] with different lipid systems, has proven the importance of lipid headgroup charge and alkyl chain saturation in assessing nanotoxicity. We have come to the conclusion that the effect of the nanoparticles will depend on where they are administered and what lipid environment they are exposed to. However, we looked only into ECN which are negatively charged and spherical in shape. Future studies would need to focus on using nanoparticles with different aspect ratios, size and possibly other physicochemical properties while also varying the lipid composition to obtain a complete biophysical understanding of lipid/nanoparticle interactions in varying lipid environments. Additionally, future studies in our group will also focus on the effect of ionic strength and the presence of ions with different valence on nanoparticle induced changes in lipid domain packing. A complete understanding of the fundamental physical principles governing lipid-nanoparticle interactions are essential in order to develop methods to predict the potential adverse effects of ENPs with varied applications.

We also observed the interaction between cholesterol and MiniB which is very specific to lung surfactant research and Surfactant Replacement Therapy. Our data revealed the potency of the synthetic protein MiniB to counter the harmful effects of cholesterol.